

8597

THERMAL NEUTRON CAPTURE IN ^{58}Fe

THERMAL NEUTRON CAPTURE IN ^{58}Fe

by

C.A. ADESANMI, B.Sc (Ife)

A Thesis

Submitted to the School of Graduate Studies

in Partial Fulfilment of the Requirements

for the Degree

Master of Science

McMaster University

December 1979

MASTER OF SCIENCE (1979)
(PHYSICS)

McMASTER UNIVERSITY
HAMILTON, ONTARIO.

TITLE: THERMAL NEUTRON CAPTURE IN ^{58}Fe

AUTHOR: C.A. ADESANMI, B.Sc. (Ife)

SUPERVISOR: Dr. T.J. KENNETT

NUMBER OF PAGES: ix, 89

SCOPE AND CONTENTS:

This thesis reports on the $^{58}\text{Fe}(n,\gamma)^{59}\text{Fe}$ reaction. The main concern has been to determine the energies of the gamma rays, measure their intensities, deduce the neutron separation energy and investigate the correlation between this reaction and the $^{58}\text{Fe}(d,p)^{59}\text{Fe}$ reaction. Previous work carried out by different groups using different reactions and techniques are reviewed, and the basic principles of the neutron capture reaction presented. The experimental facility available at McMaster University is briefly described. Gamma ray spectroscopy and details of experimental arrangement and procedure are discussed. Details of the data analysis was also discussed.

ACKNOWLEDGEMENTS

I would like to express my profound gratitude to Dr. T.J. Kennett for his superb supervision and I sincerely appreciate his guidance, which led to the successful completion of this work. I wish to thank Dr. W.V. Prestwich whose suggestions and discussions have proved useful on all occasions. I also acknowledge the contributions made by Mr. M.A. Islam, Dr. P. Brewster, Mr. N. Barkman, Dr. S. Kerr, Mr. K. Chin, Mr. U. Akano, and Mr. A. Momo to make this work a success. I am indeed grateful for the beautiful work done by Mrs. D. Matthews in typing this thesis. The University of Ife, Nigeria, and McMaster University deserve special thanks for providing the financial assistance that made this important part of my education possible.

TABLE OF CONTENTS

		<u>Page</u>
CHAPTER 1	INTRODUCTION	1
1.1	Review of previous work	1
1.2	Motivation for this work	5
1.3	Neutron capture reactions	7
CHAPTER 2	EXPERIMENTAL FACILITY AT McMASTER UNIVERSITY	10
2.1	IRRADIATION SYSTEM	10
2.1.1	McMaster Nuclear Reactor	10
2.1.2	Reactor Neutron Fluence	10
2.1.3	The internal target arrangement	13
2.1.4	Choice of capsule material	15
2.1.5	Loading system	15
2.1.6	Collimation	18
2.1.7	Background	21
2.2	GAMMA RAY SPECTROSCOPY	23
2.2.1	Gamma ray interaction with matter	23
2.2.2	The intrinsic germanium detector	27
2.2.3	The sodium iodide scintillation detector	29
2.2.4	Detector response	30

TABLE OF CONTENTS

		<u>Page</u>
2.3	SPECTROSCOPY SYSTEM	33
2.3.1	511 keV Gamma ray coincidence	33
2.3.2	Bremsstrahlung rejection	37
2.4	ELECTRONIC CIRCUITRY	37
CHAPTER 3	EXPERIMENT	40
3.1	THEORY	40
3.1.1	Energy	40
3.1.2	Intensity	47
3.2	PROCEDURE	52
CHAPTER 4	DATA ANALYSIS	60
4.1	Energy gamma rays	60
4.2	Neutron separation energy	68
4.3	Intensity determination	68
CHAPTER 5	DISCUSSION OF RESULTS	73
CHAPTER 6	CONCLUSIONS	83

LIST OF ILLUSTRATIONS

		<u>Page</u>
Figure 1.1	Total neutron cross section for Rh.	9
Figure 2.1	Reactor neutron fluence.	11
Figure 2.2	Irradiation system.	14
Figure 2.3	Sample loading in through tube.	16
Figure 2.4	Collimation system.	20
Figure 2.5	γ -ray background contribution by through tube.	22
Figure 2.6	Three primary interaction mechanisms between γ -rays and electrons in a detector.	25
Figure 2.7	Variation of absorption coefficient in Ge with energy gamma rays in different interaction and sum total effects.	25
Figure 2.8	Components of detector response to 2223 keV photons and their manifestation in a typical Ge spectrum.	32
Figure 2.9	Components of pair spectrometer response and an observed spectrum for 9 MeV photons.	35
Figure 2.10	Electronic circuitry.	39
Figure 3.1	Shows original spectrum, zero area digital filter and convolved spectrum.	44
Figure 3.2	Variation of gain with energy.	46
Figure 3.3	Illustration of peak area determination.	48
Figure 3.4	Detector efficiency curve.	50

		<u>Page</u>
Figure 3.5	Spectrum of iron isotope (^{58}Fe) in (a,b) singles mode Part 1 and Part 2.	55 56
Figure 3.6	Spectrum of iron isotope (^{58}Fe) in triple coincidence.	57
Figure 3.7	Spectrum of natural iron in triple coincidence.	58
Figure 3.8	Spectrum of Nitrogen and ^{58}Fe in triple coincidence.	59
Figure 4.1	Decay scheme of ^{59}Fe .	67
Figure 5.1	Intensity against Nilsson band.	80
Figure 5.2	Plot of intensity in ^{59}Fe vs. average intensity in the Nilsson band of ^{183}W ^{181}Hf and ^{179}Hf .	82

LIST OF TABLES

	<u>Page</u>
1. Sample isotopic analysis in enriched ^{58}Fe .	2
2. Summary of samples, materials and irradiation time.	54
3. Energies and intensities of γ -rays from the primary transitions of the reaction $^{58}\text{Fe}(n,\gamma)^{59}\text{Fe}$.	62
4. Secondary γ -rays from the $^{58}\text{Fe}(n,\gamma)^{59}\text{Fe}$ reaction.	64
5. Neutron separation energy.	66

CHAPTER 1
INTRODUCTION

1.1 Review of previous work.

Several studies on the iron isotopes have been conducted by means of (d,p), (t,p) and (n, γ) reactions. Many groups and individuals have reported results of their investigations on ^{58}Fe using different reactions and techniques. (1-2, 5-10)

The stable iron isotopes have mass numbers 54, 56, 57 and 58 and the abundances found in the nature of these isotopes are listed correspondingly in Table 1. A. Sperduto and W.W. Buechner⁽¹⁾ investigated the (p,p') and (d,p) reactions of these isotopes. They used protons and deuterons to bombard the samples of different isotopic compositions using the MIT-ONR electrostatic generator, and a 50 cm broad-range single-gap spectrograph. Their study was limited to the region between the ground state and 4.87 MeV in the case of the isotope ^{58}Fe and they were able to measure energies of some 64 levels. The Q-value measured for the ground state transition was 4.357 ± 0.008 MeV.

E.D. Klema et al.⁽²⁾ reported the detailed

TABLE 1
SAMPLE ISOTOPIC ANALYSIS
(ENRICHED IRON ^{58}Fe)

Isotope	Atomic %	Natural Abundance	Cross-section of (n, γ) reaction (barn)
54	0.67	5.8	2.25
56	20.99	91.8	2.63
57	1.80	2.1	2.48
58	76.54	0.3	1.15

The values of natural abundance are quoted from the Chart of the Nuclides by General Electric, (revised by F. William Walker et al.⁽³⁾) and the values of cross-section σ_{γ} are from Neutron Cross-section, volume I, by S.F. Mughabghab and D.I. Garber.⁽⁴⁾

measurements of the absolute cross-sections for the (d,p) reaction for the ground state and seven excited states of ^{59}Fe . They deduced values of the orbital angular momentum transfer and spectroscopic factors, and assigned spins by use of the empirical J-dependence rules. The assignments were $(E_{\text{exc}}, \ell, J, S) = (0, 1, 3/2, 0.45)$ for ground state and excited states as $(0.287, 1, 1/2, 0.22)$, $(0.470, 3, 5/2, 0.54)$, $(0.728, 1, 3/2, 0.20)$, $(1.025, [3], [7/2], 0.08)$, $(1.214, 1, 1/2, 0.81)$, $(1.572, 4, 9/2, 1.07)$ and $(1.749, 2, 5/2 [3/2], 3.59/(2J+1))$.

Another group, K.C. McLean et al.⁽⁵⁾ investigated the level structure of ^{59}Fe using the (d,p) and (t,p) reactions. They assigned spins to a large number of levels in ^{59}Fe from the comparison of the angular momentum transfer of the two reactions and carried out measurements of the cross-sections for the one and two neutron stripping reactions. They also reported that their experimental data strongly support the existence of rotational band structure in ^{59}Fe .

The spectrum of the γ -rays from the reaction $^{58}\text{Fe}(n, \gamma)^{59}\text{Fe}$ was first investigated by A.P. Bogdanov et al.⁽⁶⁾ with the aid of a coincidence spectrometer which embodied NaI(Tl) detectors. Two years later A.P. Bogdanov and

another group⁽⁷⁾ studied the spectrum of γ -rays emitted upon capture of thermal neutrons by ^{58}Fe using a Ge(Li) spectrometer. Energies and intensities of transitions were determined and a decay scheme was proposed by them. The Ge(Li) detector they used had a sensitive volume of about 3 cm^3 which is rather small and a poor resolution of 10 keV at E_γ of 1 MeV, and 30 keV at E_γ of 6 MeV, thus limiting the quality of the data. The error incurred in the determination of the energies of γ -rays ranges between 3 to 6 keV. The intensities they reported were in percent per neutron capture in ^{58}Fe and based upon an assumed cross-section.

E.K. Warburton et al.⁽⁸⁾ formed ^{59}Fe via $^{48}\text{Ca}(^{15}\text{N}, 3np)^{59}\text{Fe}$ and $^{48}\text{Ca}(^{18}\text{O}, 3n\alpha)^{59}\text{Fe}$ reactions. They identified γ -rays associated with ^{59}Fe from the relative intensities observed as a function of both energy and type of projectile. Their work confirmed some spin-parity values assigned to some levels in works previously reported but they suggested a spin-parity $5/2^-$ for the 571 keV level which does not agree with $3/2^-$ assigned by McLean.

A recent work on $^{58}\text{Fe}(n, \gamma)^{59}\text{Fe}$ was carried out by R. Vennink et al.⁽⁹⁾. They measured circular polarization of γ -rays from the capture of polarized neutrons in

isotopically enriched targets of ^{58}Fe . The circular polarization of γ -rays resulting from the capture of polarized thermal neutrons is related to the spin of the final state. The measurement of the degree of circular polarization enabled them to assign spins to some levels. They were $(E_x, J^\pi) = (1921, 3/2 | 5/2^+)$, $(1962, 1/2^-)$, $(2445, 3/2 | 5/2^+)$.

J.C. Wells, Jr. et al.⁽¹⁰⁾ carried out a series of neutron capture γ -ray measurements following resonance capture in enriched ^{58}Fe . They observed twenty-eight γ -rays (8 primary and 20 secondary) from two resonances of the $^{58}\text{Fe}(n, \gamma)^{59}\text{Fe}$ reaction and placed nineteen of them into a level scheme for ^{59}Fe . Photon energies in the reaction were measured and their intensities determined. They deduced ^{59}Fe resonances, and also the levels and neutron separation energy which they reported as 6580.8 ± 1.0 keV.

1.2 Motivation for this work.

Energies of gamma rays obtained to a high degree of accuracy have been found useful in various ways. Among other things, according to D.E. Alburger⁽¹¹⁾, they can be used to determine excitation energies of nuclear

states, measurement of Q-values and for calibration of resonance energies. These can in turn lead to the determination of accurate atomic masses.

Knowledge of the energy of gamma rays of ^{58}Fe has proved useful in solving an interference problem encountered in a recent determination of the isotopic ratio in a lunar sample. Furthermore, in the field of nuclear medicine and biophysics this reaction could be useful.⁽¹²⁾ M.A. Kaplan et al.⁽¹³⁾ studied the assimilation of ^{59}Fe in patients with cancer of the stomach.

In the present thermal neutron capture reaction studied, gamma rays of high energies in the range of 4 MeV to 8 MeV were specifically examined by means of intrinsic germanium-sodium iodide pair spectrometer of high sensitivity. The lower energy gamma rays were examined using anti-coincidence circuitry. The detector resolution is less than 6 keV in the range of energy gamma rays under consideration. This is much better than the 10 to 30 keV detector resolution used in one of the previous works. The energy of the gamma rays was determined more accurately than previously and the intensities are more reliable. The Q-value was also obtained from the sets of cascades of gamma rays detected.

1.3 Neutron Capture Reactions.

When a thermal neutron is captured by a nucleus the resulting compound nucleus is left in an excited state. For example, the thermal neutron capture reaction in the iron isotope ^{58}Fe may be written as



The energy Q is released in the reaction. The energy of the thermal neutron is about 0.025 eV. The energy released is the Q -value and it is the same as the binding energy of the last neutron in the product nucleus.

The nucleus may de-excite from the capture state by emission of a photon or a cascade of photons. The resulting capture gamma ray spectra are generally complex. They consist of both low and high energy gamma radiations. The life-time of the capture state is typically 10^{-14} seconds and photons emitted are referred to as prompt gamma rays. In neutron capture gamma ray analysis, irradiation of the sample and the measurement of the radiation are performed simultaneously. (14-15)

The rate of neutron capture reaction depends on the cross section of the target nuclide and the neutron flux. The rate per isolated atom of the (n,γ) is

$$R(\underline{r}) = \int_0^{\infty} \phi(E, \underline{r}) \sigma(E) dE.$$

$\sigma(E)$ is the cross section of the target nuclide. It is a measure of the probability of the reaction occurring for a given incident neutron energy. It is measured in barns ($1 \text{ barn} = 10^{-24} \text{ cm}^2$). In the thermal region, where the energy of a neutron is a fraction of an electron-volt, the cross section $\sigma(E)$ varies as $1/\sqrt{E}$. In this low energy region there are resonances also. A resonance will occur when the energy of the neutron together with mass-energy of the target equals a quantum energy level of the product nuclide. Figure 1.1 shows the variation of cross section $\sigma(E)$ in low energy region. $\phi(E,r)$ is the particle neutron flux. It is usually defined as a number of neutrons of thermal energy incident on a unit area at a position r , per unit time.

Energies of the emitted photons depend on the energy levels of the product nuclide. Therefore each nuclide will display a unique gamma ray spectrum after neutron capture. It is this spectrum that is used in analysis which lead to the measurement of energies of these gamma rays and their intensities.

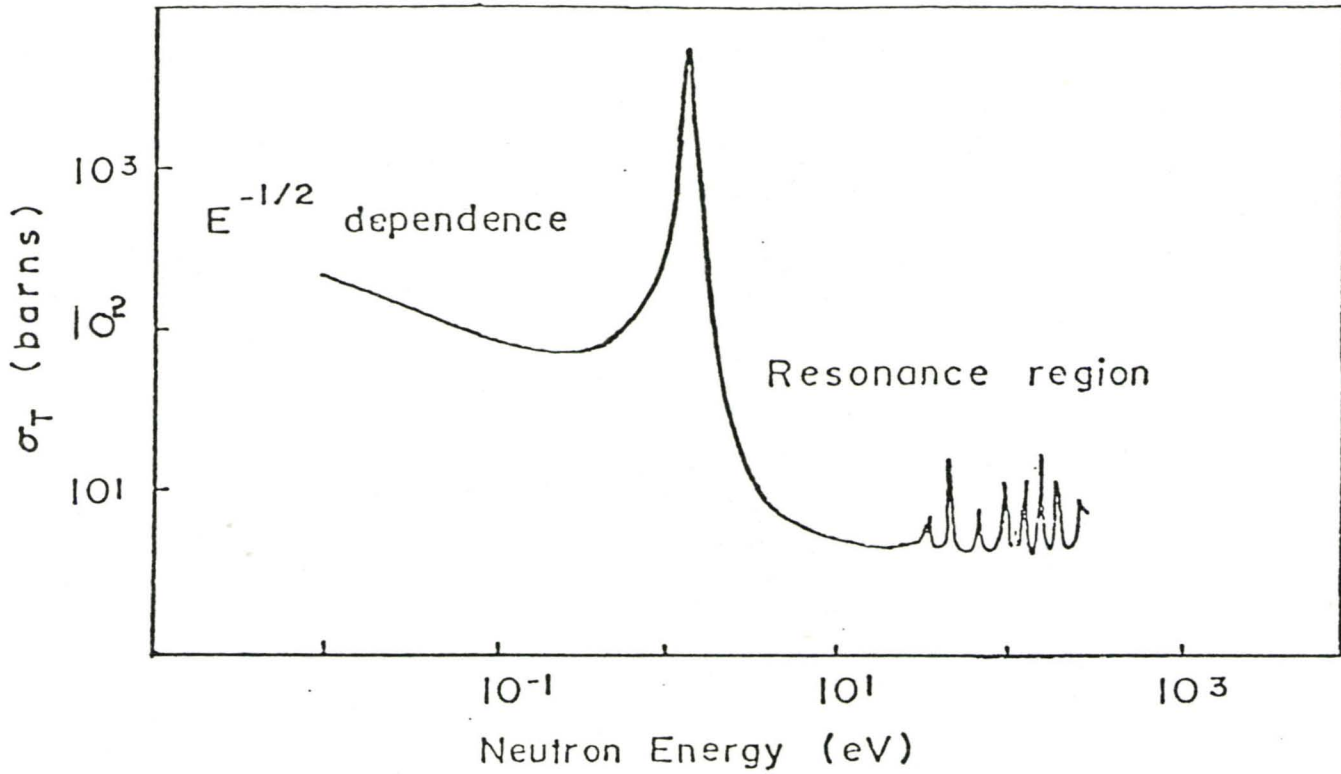


Figure 1.1 Total neutron cross section for Rh. Although elastic scattering is included, the (n, γ) reaction is by far the larger component.

CHAPTER 2

EXPERIMENTAL FACILITY AT McMASTER UNIVERSITY

2.1 IRRADIATION SYSTEM

2.1.1 McMaster Nuclear Reactor

McMaster University has a light water-moderated pool type of a nuclear reactor. It is designed for research purposes and it provides neutrons for irradiation of samples under study. The fast neutrons produced from fission are moderated to thermal energies. It has a core loading capacity of 5.0 kg of uranium enriched to 90% ^{235}U . The reactor can operate at a maximum power level of 5 MW thermal but during the irradiation of the isotope ^{58}Fe , it was operating at 2 MW thermal. The average core neutron particle flux was approximately $2 \times 10^{13} \text{ n/cm}^2/\text{s}$ but at the sample position the flux has reduced by a factor of ten, and thermal neutron flux was of the order of $10^{12} \text{ n/cm}^2/\text{s}$. The water of the pool serves not only as a moderator, it cools the reactor and acts as a shield.

2.1.2 Reactor Neutron Fluence

Figure 2.1 shows flux distribution in a nuclear reactor. The neutron fluence is a function of energy which may be divided into three main regions. They are

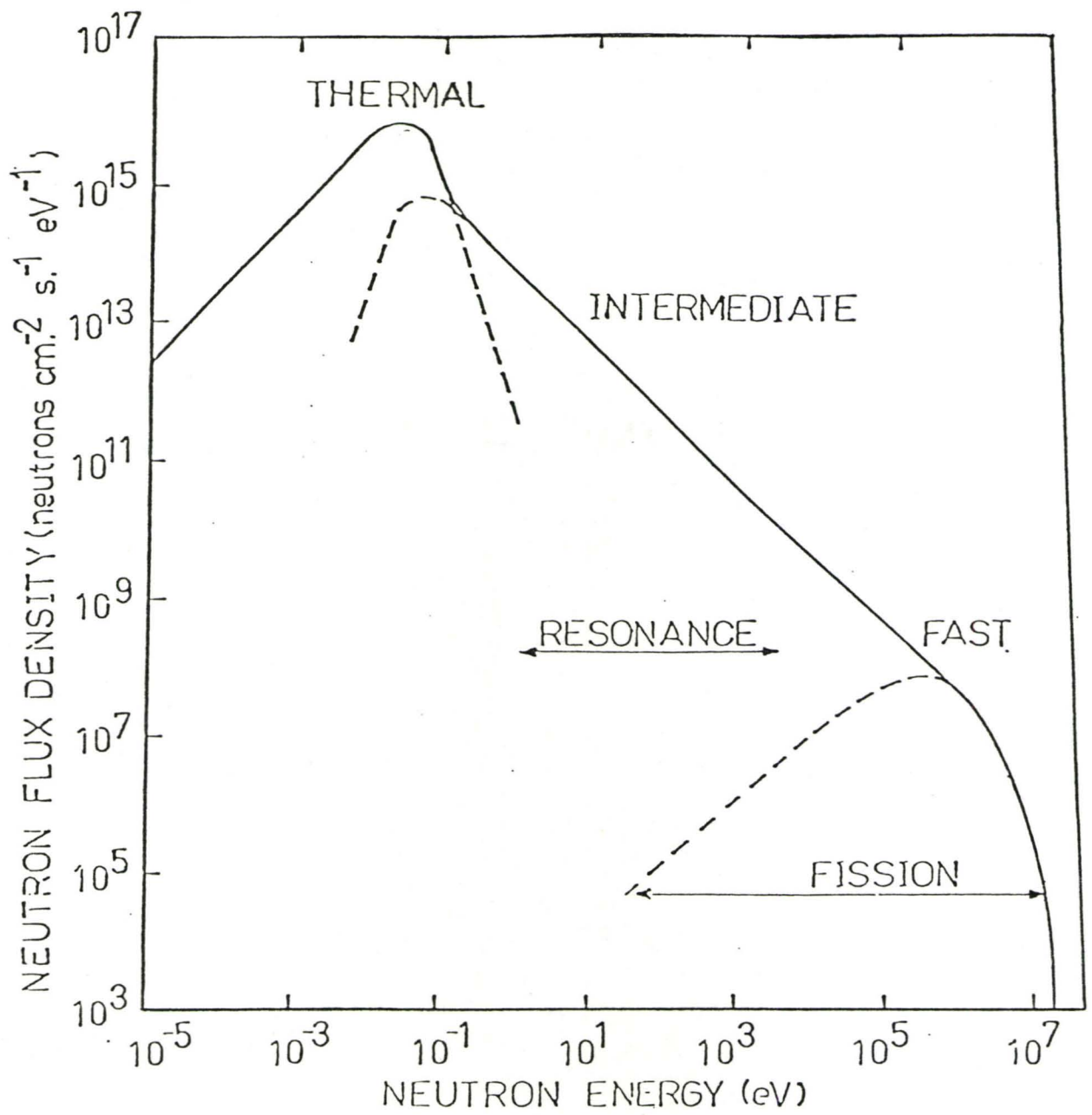


Figure 2.1 REACTOR NEUTRON FLUENCE

the thermal region, intermediate region, and the fast region. In the thermal region the neutron energy is a fraction of electron-volt, the energy is between 1 eV and 0.1 MeV in the intermediate region and for the fast region the energy is greater than 0.1 MeV. The flux exhibits a sort of a Maxwellian distribution in the thermal region with the flux being proportional to $Ee^{-E/KT}$

$$\phi(E) \propto E \exp(-E/KT).$$

E is neutron energy at absolute temperature T and K is Boltzmann constant.

The intermediate region which is the slowing down region has a flux which varies as $1/E$

$$\phi(E) \propto 1/E .$$

This region is also characterized with some depressions when flux varies as $1/\Sigma_a$ and it is normally referred to as the resonance region.

The fast region consists of, predominantly, a fission neutron spectrum. This is represented by a semi-empirical flux function of energy of the form

$$\phi(E) = K\sqrt{E} \exp(-E/1.29) \quad (E \text{ in MeV}).$$

Generally one can say that flux density varies as $1/E$ but in the thermal region flux density is maximum. This is to say that most of the neutrons are thermal neutrons.

2.1.3 The internal target arrangement

The McMaster nuclear reactor contains a facility where samples can be irradiated in the "through tube". Figure 2.2 shows the horizontal tangential tube. This tube is made of aluminum because this material does not react with the pool water nor does it deteriorate in the areas of high neutron flux. The concrete block is the wall of the reactor and it stops radiation from getting into the experimental zones. The internal target arrangement is most advantageous in the sense that the high flux at the sample position could result into maximum counting rate for a small sample. This can be clearly understood by considering the geometrical set up. In this case, the system suffers a diminishing counting rate due to only one solid angle. This is the angle the gamma ray detector subtends at the target. In the case of external-target arrangement, there is more diminishing counting rate due to an additional solid angle which the neutron source subtends at the target. (16)

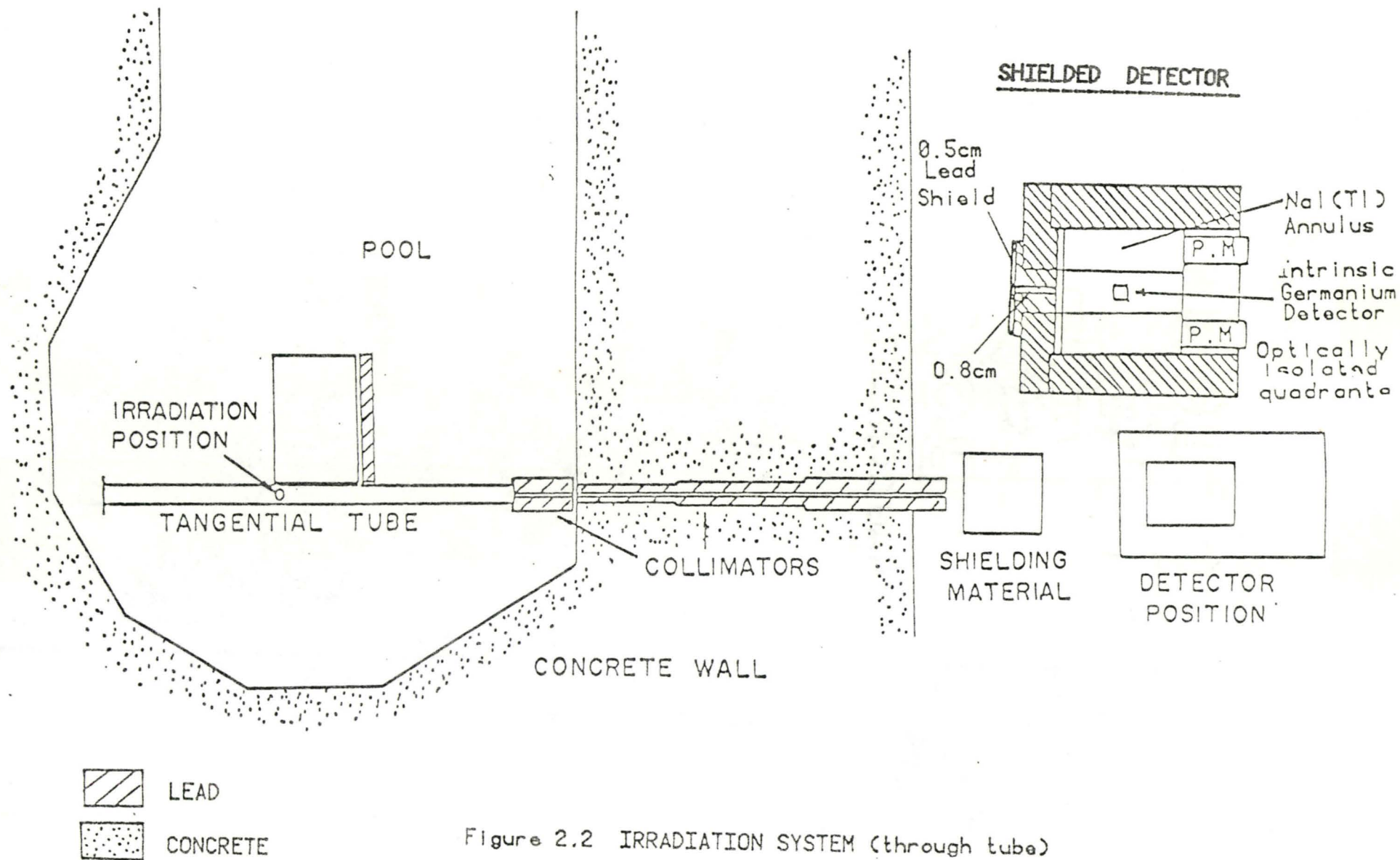


Figure 2.2 IRRADIATION SYSTEM (through tube)

Also the positioning of the target within the reactor leads to a much improved sensitivity and hence a better signal-to-noise ratio is obtained⁽¹⁷⁾. In addition, the resultant gamma rays beam can be well collimated.

2.1.4 Choice of capsule material

The choice of material of the capsule used is such that it is not much radioactive after irradiation for easy handling, and it is easily machined. The beryllium capsule contributed a minimum background to the spectrum obtained from the (n, γ) reaction and no interference with the peaks from the isotope considered. The peaks are spaced in the energy range between 0 to 7 MeV, so that their known gamma rays energies may be used as checks for our calibration. The size of the beryllium capsule is small and it was specially designed to suit the small size of the sample which is 10 mg of enriched iron isotope, ^{58}Fe .

2.1.5 Loading system

The device consists of a P.V.C. flexible tube 10 m long by 2.5 cm in diameter stretching from the pool surface to the tangential tube. Figure 2.3 shows the irradiation loading system. The sample in a small beryllium capsule with graphite top, as in the case of the ^{58}Fe , was

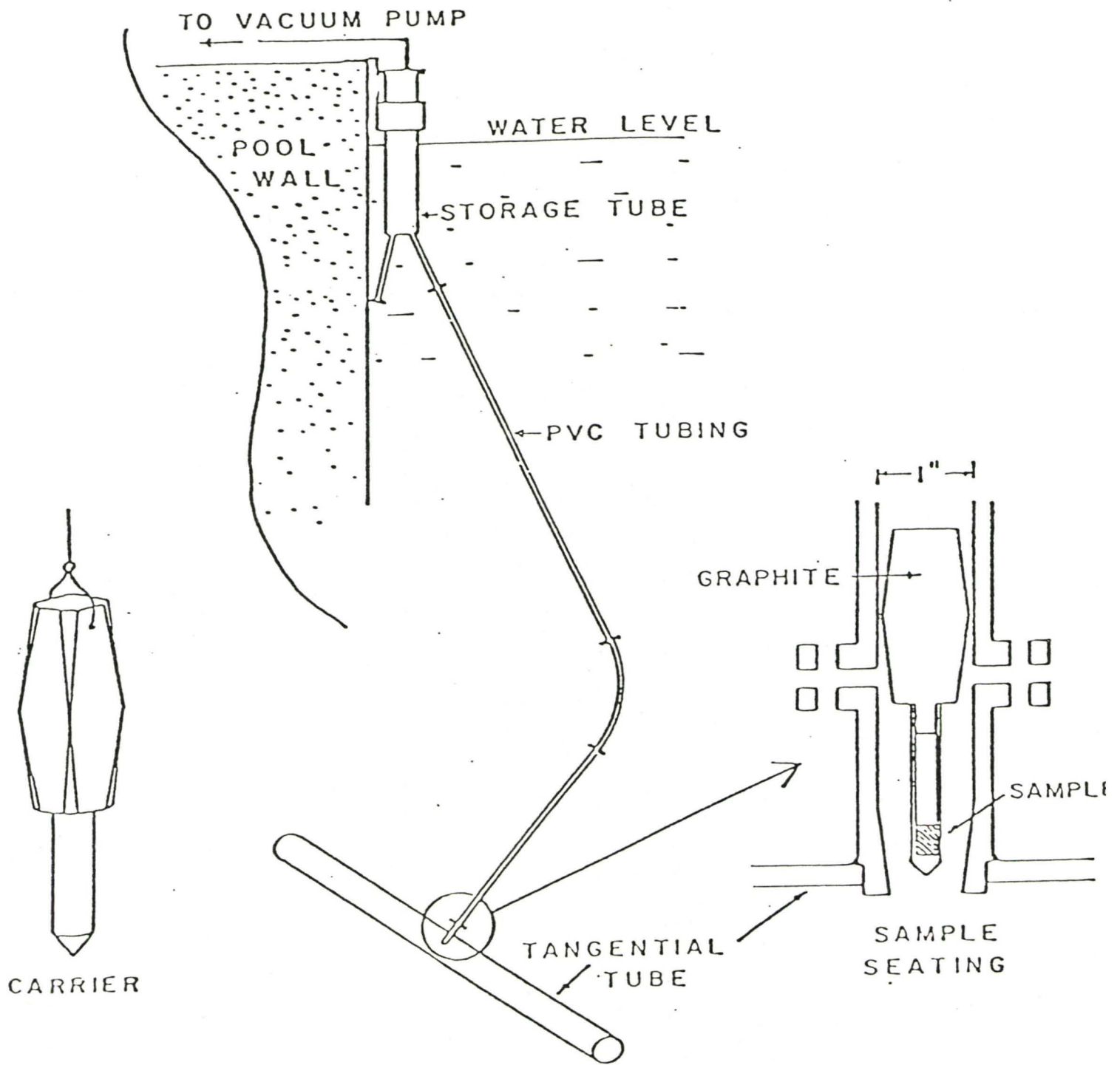


Figure 2.3 SAMPLE LOADING IN THROUGH TUBE

lowered into the irradiation position using a flexible aluminum chain attached to a nylon line, both up to 10 m long. This irradiation position is near the core and the flux at this position is a factor of 10 less than at the centre of the core. On the average, when the reactor is operating normally at 2 MW thermal, the neutron particle flux at the sample position is of the order of 10^{12} n/cm²/s.

After the target has been put in the irradiation position, the through tube is sealed with a circular aluminum plate and tightened down with four strong and well spaced screws. The tube is evacuated to a pressure of about 20 - 30 torr, and the evacuation is maintained throughout the experiment. This is to reduce a potential hazard to health or operation. Gases may be evolved from the reaction thus building up pressure in the tube and nitrogen or air contents may act as impurities in the spectrum.

The sample is removed the same way it was inserted. When the sample is removed from the irradiation position it is kept in the storage tube which is a little below the surface of the pool. If the activity of the irradiated

sample was too high, the sample was first drawn half-way up in the through tube and the activity is allowed to drop to a few mR/sec before it was raised fully, and placed in the storage tube. While in the storage tube, the activity was allowed to drop to a level which could not cause a health hazard. The sample is then removed and kept behind bricks in the reactor building.

The major advantage of this loading system is that the reactor need not be shut down when the target is inserted or removed from irradiation position. When the reactor is in operation, no radiation is issued out from the opened tube.

2.1.6 Collimation

This internal-target arrangement requires fine collimation of the beam and extensive shielding of the beam port. To achieve this, the collimation system was constructed in three different subsections.

First there is an evacuated aluminum target chamber. The ends of the target chamber are well removed from the high flux and they are machined in the central region to 1.6 mm.⁽¹⁷⁾ This helps to minimize background radiation produced by neutron capture in aluminum

through $^{27}\text{Al}(n,\gamma)^{28}\text{Al}$ reaction. The sample chamber is fabricated from 7.6 cm O.D. 65 ST aluminum tubing and is approximately 2 m long.

There is another internal collimation system built in the pool and a neutron absorption assembly. The internal collimation system consists of a 15.2 cm diameter, 23 cm long lead annulus with a 3.8 cm aperture. (17) There is a neutron absorption assembly which removes thermal neutrons from the gamma ray beam. This section is aligned with the external collimator.

The external collimator is 190 cm long with a 1 cm diameter aperture. A 50 cm lucite rod in the collimator shields the germanium detector from fast neutrons (18). Figures 2.2 and 2.4 illustrate the essential features of the collimation system. There is a slab of paraffin wax which is placed in the beam path to attenuate the fast neutrons before getting to the germanium detector. In addition, the wax can be used to regulate the intensity of the gamma ray that gets to the detector.

What is most important is that the collimation prevents gamma rays from the (n,γ) reaction from getting directly to the sodium iodide detector. The γ -rays beam is made to impinge on the germanium detector only.

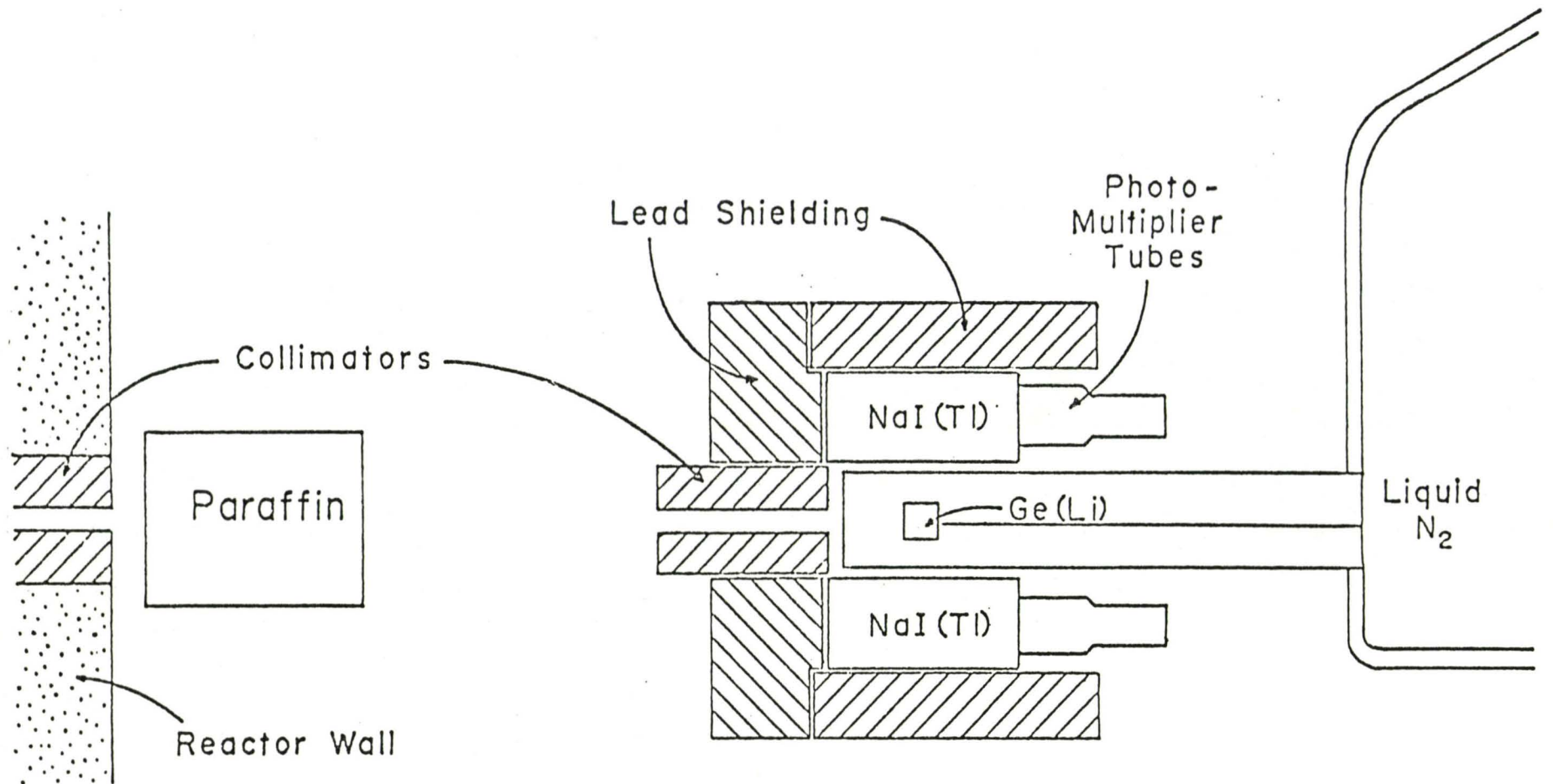


Figure 2.4 COLLIMATION SYSTEM

2.1.7 Background

Several sources of radiation can be identified in the observed background. The influence of gamma rays from the reactor is itself relatively unimportant. The main source of background in our experiments has been caused by neutron-capture gamma rays emitted from various structural components of our experimental system. The background radiation is a continuum with strong components at two energies, 2223.7 keV gamma ray due to $H(n,\gamma)D$ reaction and 7725.7 keV ground state transition from $^{27}Al(n,\gamma)^{28}Al$. The former may be due to the pool water at the end of the through tube. The target chamber is made of aluminum, so the latter reaction may be due to the presence of aluminum of the end plate of the through tube. Figure 2.5 shows the gamma ray background contribution by the through tube itself. (19)

In addition, ^{41}Ar and ^{60}Co lines were detected when the experiment was carried out in a singles mode. These lines must have been due to the presence of Argon in the air and ^{60}Co present in the reactor.

LOG₁₀ COUNTS

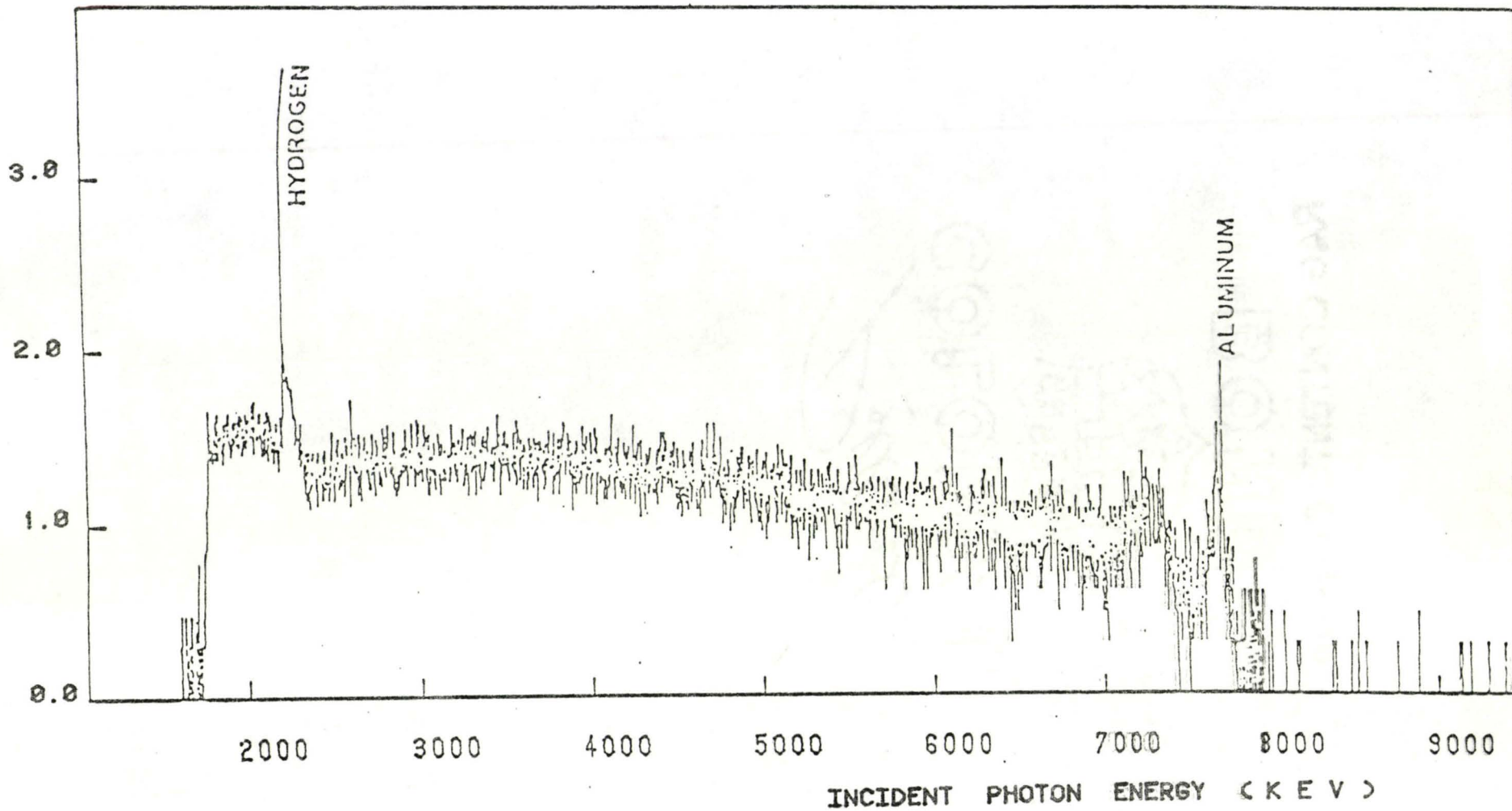


Figure 2.5 γ -ray background contribution by through tube

2.2 GAMMA RAY SPECTROSCOPY

Details of gamma ray spectroscopy will not be discussed but it is pertinent to briefly discuss the gamma ray interactions with matter and the detection system.

2.2.1 Gamma ray interaction with matter.

In neutron capture gamma rays analysis, the product nucleus is in an excited state and decays with emission of prompt gamma rays. The detection of these gamma rays and the determination of their energies, lead to determination of the energy levels of the excited nucleus. Gamma ray detection can be accomplished by identifying the various ways they interact with matter. Three major types of interactions are noticeable. They are photoelectric effect, Compton scattering and positron-electron pair production. The overall effect depends on the sum of the cross-sections of these three mechanisms.

In the photoelectric effect, the photon interacts with an atom in such a way that its total energy is given to an electron which is expelled from the atom. The probability of K electrons being involved is highest when the photo-energy is equal to the K electron binding energy and at energy higher than the K absorption edge. According

to H. Hall (20)

$$\sigma_{\text{ph}} (K) = \frac{32\pi\sqrt{2}}{3(137)^4} Z^5 \left(\frac{m_0 c^2}{h\nu}\right)^{7/2} .$$

The dependence of cross-section σ_{ph} on the fifth power of atomic number Z holds for all energy ranges considered in this project. Figure 2.6 illustrates the three main interactions in the detector taken from Richard H. Pehl's article (21).

A photoelectric event produces an amount of ionization which is directly proportional to the gamma rays energy, while the Compton event produces a variable amount of ionization. The Compton effect is due to a scattering process between the photon and a free atomic electron. The gamma rays are not absorbed completely but scattered sometimes in the forward direction with less energy transferred. The Compton scattering cross-section per electron was first calculated by Klein and Nishina (22) as

$$e\sigma_c = 2\pi r_e^2 \left\{ \frac{1+\gamma}{\gamma^2} \left[\frac{2(1+\gamma)}{1+2\gamma} - \frac{1}{\gamma} \ln(1+2\gamma) \right] + \frac{1}{2\gamma} \ln(1+2\gamma) - \frac{1+3\gamma}{(1+2\gamma)^2} \right\}$$

where $\gamma = h\nu/M_0 c^2$ represents the "reduced" incident γ energy and the total collision cross-section is obtained by integration over all scattering angles. (Physics of Nuclei and Particles - Pierre Marmier and Eric Sheldon).

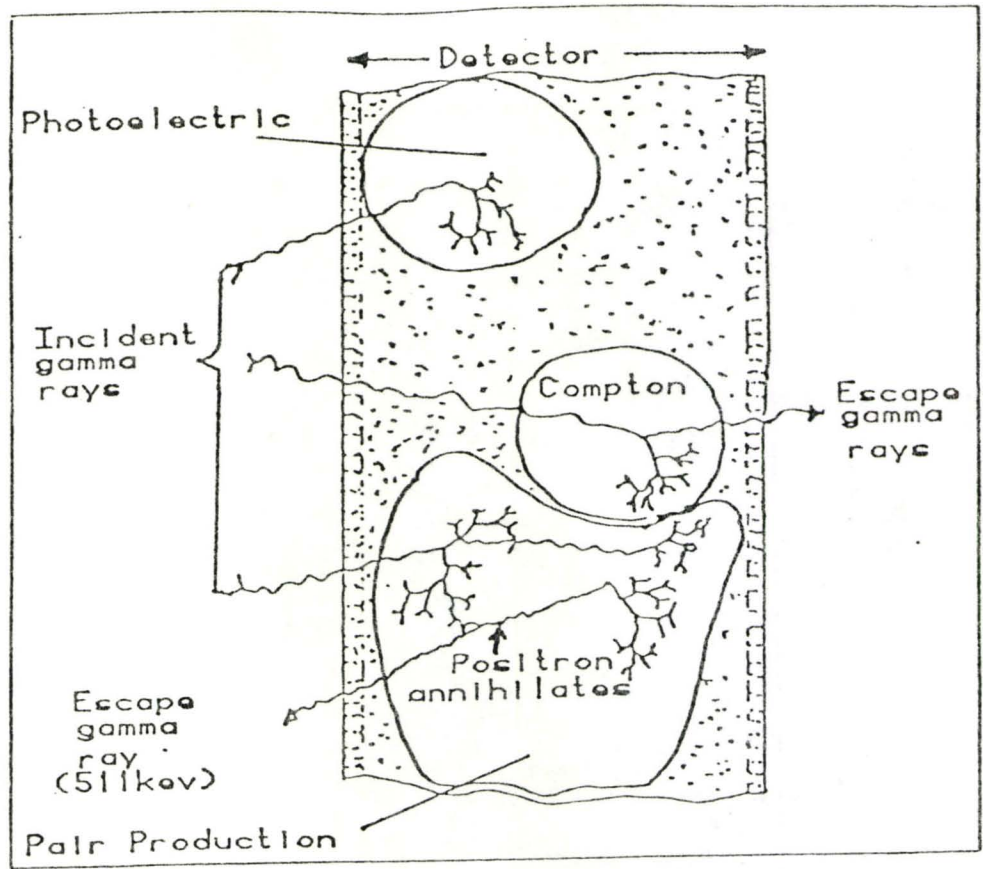
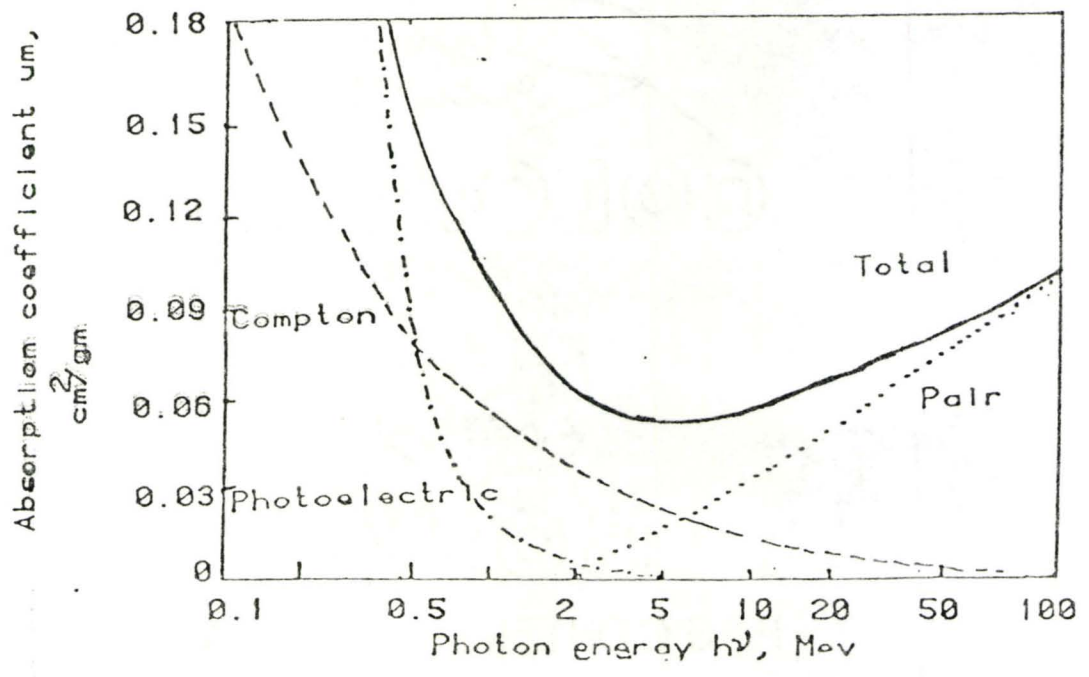


Figure-2.6 THREE PRIMARY INTERACTION MECHANISMS (between γ -rays and electrons in a detector).
 Figure 2.7 VARIATION OF ABSORPTION COEFFICIENT IN GE. (with energy gamma rays in different interaction and sum total effects).



For an atom the total cross section is

$$\sigma_c (\text{atom}) = Z \cdot \sigma_c .$$

From the consideration of the dynamics of the interaction it can be shown that the energy of the scattered photon, E , is given by

$$E = \frac{E_0}{1 + \left[\frac{E_0}{M_0 C^2} \right] [1 - \cos\theta]}$$

where θ is the scattering angle.

In the case of pair production, electron-positron pairs are created with total energy equal to the energy of the photon. For this to occur, the energy of the photon must exceed $2 M_0 C^2$ which is the rest mass of the two particles, positron and electron. The cross section for pair production which is a measure of the probability that γ -rays will experience such an interaction is proportional to the square of atomic number Z ,

$$\sigma_{pp} \propto Z^2 .$$

Pair production is a result of γ -ray interaction which takes place in the field of a nucleus. The nucleus does

not experience a change of state and no atomic electron, as in the other two interactions, is involved except that the nucleus absorbs some of the momentum of the photon. Also it can not take place in a free space because conservation of energy and momentum can not be simultaneously satisfied. Figure 2.7 shows variation of absorption coefficients with energy gamma rays in the different interactions, and sum total effect of the interactions.

2.2.2 The intrinsic germanium detector.

Gamma rays emitted following thermal neutron capture in the experimental target were examined by means of a high sensitive intrinsic Ge-NaI(Tl) pair spectrometer. (23)

The germanium detector is a semi-conductor gamma ray detector. It was intrinsic and contained no doping of comparative impurity as that commonly used in the lithium drifted detector. It is a piece of solid material where electrons and holes are created as a result of absorbed gamma rays. These charge carriers are collected with the aid of an electric field applied to the material

and an electric signal which is a measure of the energy of the gamma rays, is generated.

The intrinsic germanium detector has an active volume of 28.3 cm^3 , fabricated by PRINCETON GAMMA TECH. Inc. This active volume is preferred because of its high efficiency. A small active volume detector may have high resolution but will often have low probability of gamma ray interaction in the small volume. Also there is high probability of secondary electrons escaping detection when the incident gamma ray energy exceeds 1 MeV.⁽²⁴⁾ However, the detector active volume should not be too large because the annihilated quanta may be absorbed within the detector.

A voltage of about 3000 V is applied to obtain charge collection from the whole of the detector. It is operated at low temperature with the aid of liquid nitrogen to reduce the leakage current flowing through the material.

The choice of an intrinsic germanium detector is advantageous because it is tolerant to warm up unlike germanium lithium drifted detectors.

2.2.3 The Sodium Iodide Scintillation Detector.

Many materials luminesce under the influence of nuclear radiation and this property has found wide application in gamma ray detectors. Sodium iodide "activated" with small amounts of thallium is a commonly used scintillation compound. Such detectors are extremely versatile as they can be manufactured in a variety of sizes and shapes.

A 15 cm long NaI(Tl) annulus was used. The internal diameter of the annulus is 7.5 cm and the outer diameter is 22.5 cm. The crystal is optically divided into four quadrants in order to enhance effectiveness in a pair spectrometer configuration. Each NaI(Tl) quadrant is optically coupled to a photomultiplier tube which has sufficient gain to produce a pulse of several volts on the collector.

The use of NaI(Tl) annulus is significant in a pair spectrometer. When the central Ge detector receives the kinetic energy from the electron-positron pair, two of the NaI(Tl) quadrants are used to detect the oppositely directed annihilation quanta and the

other two quadrants are used to detect the bremsstrahlung photon which may be rejected by anti-coincidence techniques.

Sodium iodide detectors have been widely used because of the fast response; they have a dead time of about 2.5×10^{-8} sec. More important is the presence of the element iodine, with a fairly high atomic number, Z , in NaI(Tl). It gives the detector a great stopping power for gamma rays. This is why it is more useful as a counter for high energy photons than any other counter. Moreover, the size of the output pulse is closely proportional to the energy quantum, hence, with the aid of a pulse analyzer, gamma rays of different energies can be separated and counted.

2.2.4 Detector Response.

When monoenergetic photons are incident on a detector, one expects that each photon will deposit all its energy in the detector, but this is not so. As a result of this, energy spectrum which is

supposed to be a delta distribution at the incident energy, takes another shape; see Figures 2.8 and 2.9. Since the production of an electron-hole pair in a germanium and scintillation photon in a sodium iodide detector, is purely statistical, the response function is a Gaussian distribution when convolved with electronic noise contribution.

Resolution is generally defined as full width at half maximum (FWHM) of a Gaussian peak. A germanium detector has a higher resolution because energy required to produce an electron-hole pair is less than that required to produce a scintillation photon in a sodium iodide detector. On the other hand, a sodium iodide detector is much more efficient than a germanium detector. It can be made much larger than any available germanium detector.

The non-ideal detector response is not due to the finite resolution only. When a photon gets into

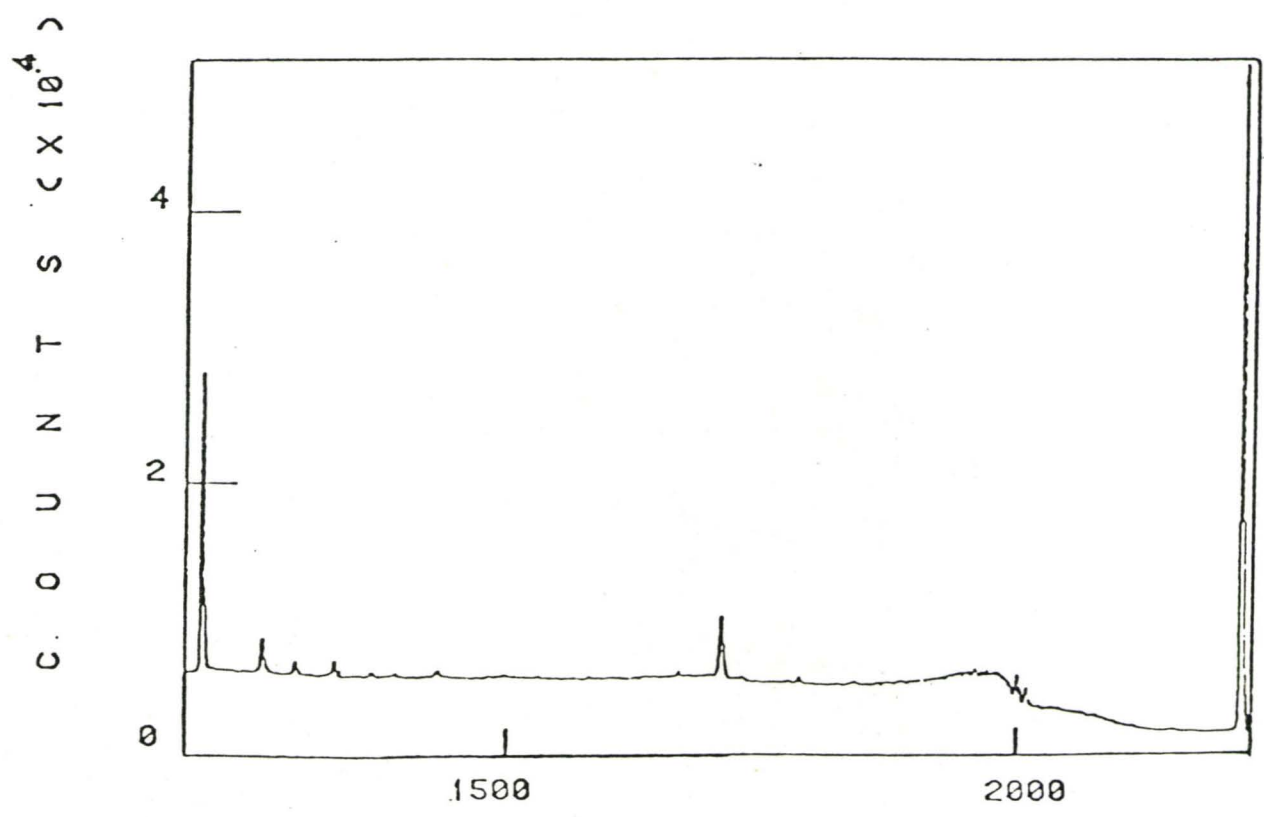
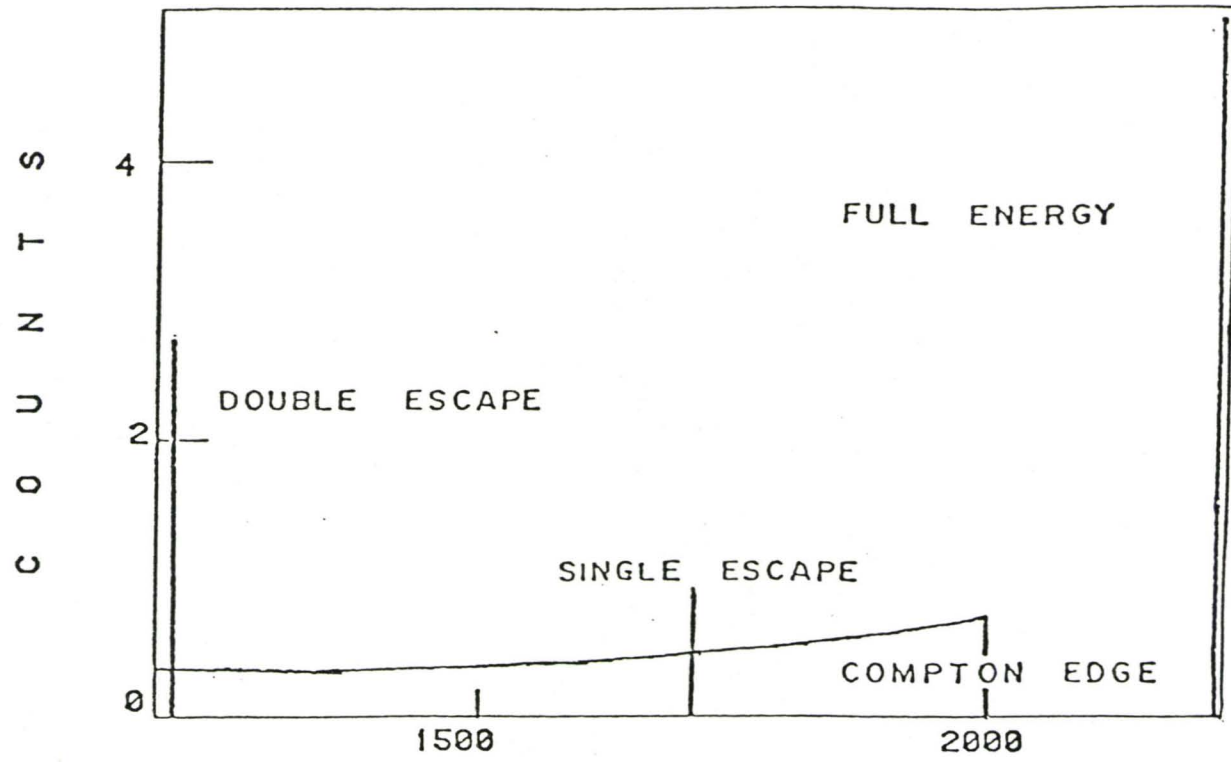


Figure 2.8 COMPONENTS OF DETECTOR RESPONSE TO 2223 KEV PHOTONS AND THEIR MANIFESTATION IN A TYPICAL GE SPECTRUM

a detector, it may be Compton scattered giving part of its energy to an electron. If the scattered photon leaves the crystal or not, the electron can have any energy between zero and the maximum value. This gives rise to a continuum in the spectrum from zero to the characteristic Compton edge. Many attempts have been made to improve this detector response and efficiency. They will be discussed in the next section. Figure 2.8 shows the detector response.

In the germanium detector, two oppositely directed quanta are formed as a result of the electron-positron pair annihilation. If they are both detected, the detector response will show a full energy peak. On the other hand, if one or both of these annihilation quanta escape, there will be a single-escape peak 511 keV below the full energy peak and a double-escape peak 1022 keV below the full energy peak.

2.3 SPECTROSCOPY SYSTEM

2.3.1 511 keV Gamma Ray Coincidence.

This system, the experimental set-up, is designed to improve the detector response which is far from ideal

and to simplify the response function which is complex. This was achieved by discriminating against all interactions and accepting pair production. A pair of the sodium iodide **quadrant** were used to indicate the presence of the two 511 keV photons which resulted from the electron-positron annihilation. In this way, the continuum due to Compton interaction was reduced and the full energy and single-escape peaks were suppressed. It was discovered that this affected the counting rate. The counting rate decreased by a factor of ten. However, the loss of efficiency in this way is compensated by the background reduction and the improvement in the signal-to-noise ratio.

The spectrum in Figure 2.9 shows that despite the set conditions, the response function is still not perfect. This is as a result of one or two annihilated gamma rays interacting in an unusual way in the **germanium detector**. This leads to the response function of the pair spectrometer deviating from the ideal one. This usually causes a "tail" with a "dip" just before a peak, and a "toe" on the high energy side of the peaks. (25) Range effect, Bremsstrahlung and Compton scattering of the annihilation quanta have

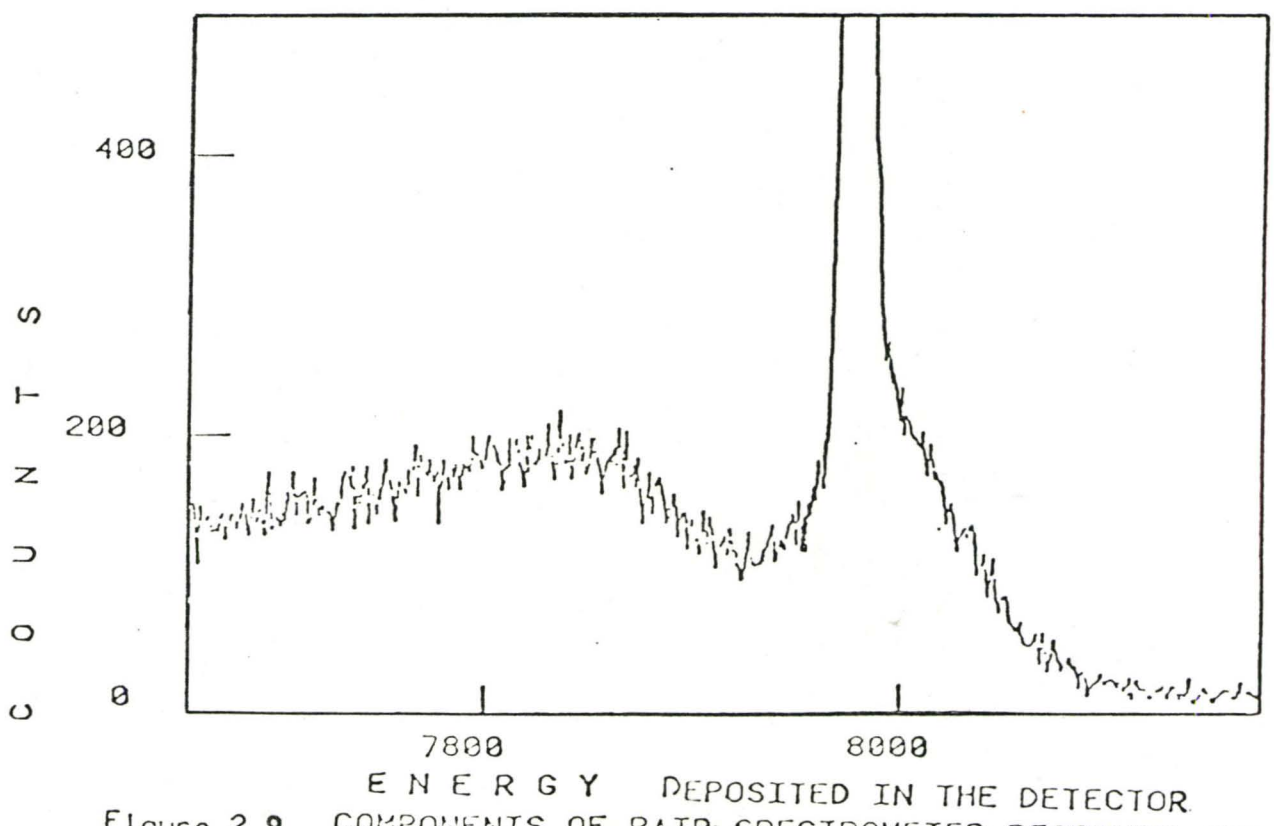
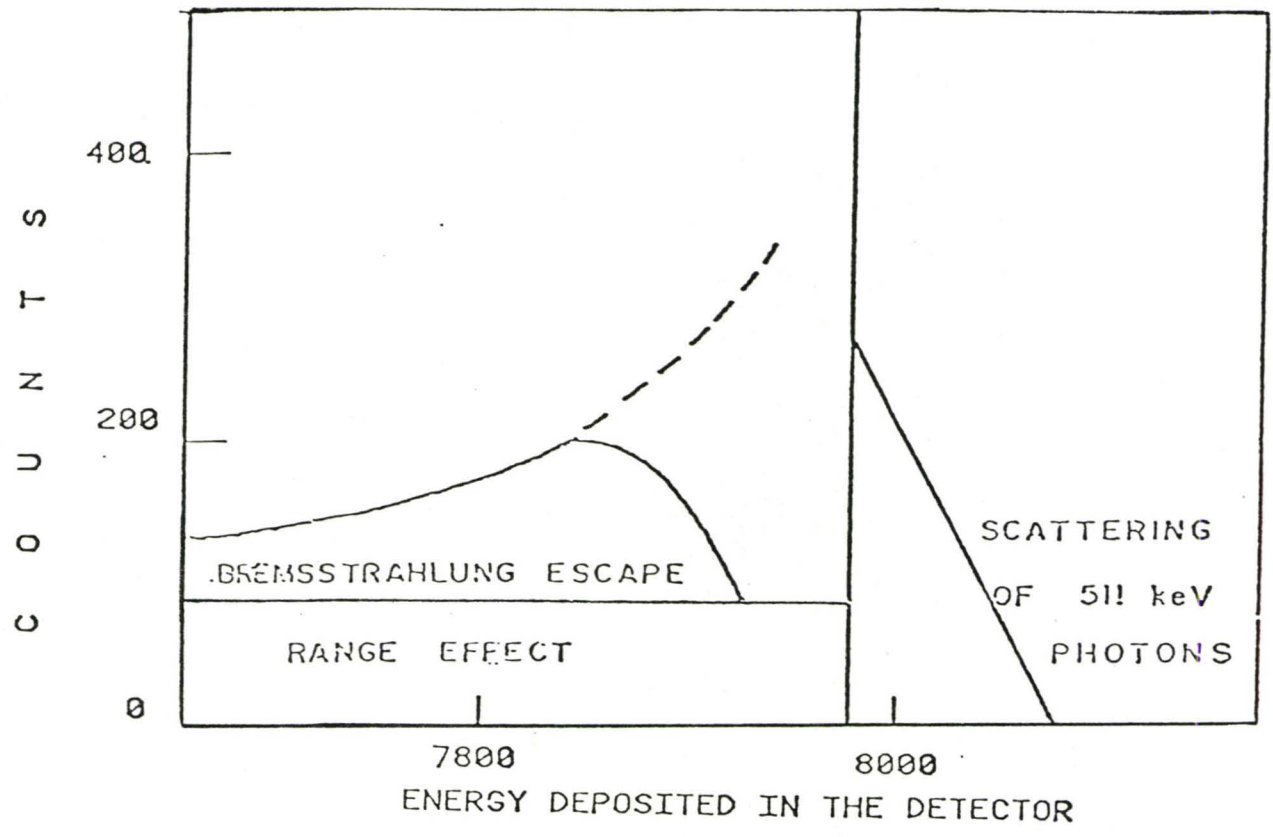


Figure 2.9 COMPONENTS OF PAIR SPECTROMETER RESPONSE AND AN OBSERVED SPECTRUM FOR 9 MEV PHOTONS.

been employed in the explanation of the presence of the tail, dip and toe on the sides of a peak. Figure 2.9 is an illustration of these defects on a particular peak.

Range effect is considered to be a result of one of the pair product, electron or positron, escaping from the active volume of the detector depositing energy less than $E_0 - 2M_0c^2$. This leads to a broad, flat continuum ranging from 0 to $E_0 - 2M_0c^2$.

Bremsstrahlung involves the slowing down of positron and electron and the radiation resulting from the slowing down. This explains why there is a tail beside a peak. When positron and electron are slowed down, they radiate electromagnetic energy. The energy deposited will be less than $E_0 - 2M_0c^2$ if the radiation is not detected. Also absorption of low energy bremsstrahlung which is unlikely to escape the germanium crystal is responsible for the dip.

The toe is a result of Compton scattering of annihilation quanta. If an annihilation quantum leaves part of its energy in germanium crystal after suffering a Compton scattering and it can still trigger a pulse, then energy greater than $E_0 - 2M_0c^2$ is deposited in the

detector causing a toe on the high energy side of a peak.

Most of these defects, except the toe, can be helped. The toe is due to an inherent poor resolution of a sodium iodide detector. The tail is reduced with the use of electronic set up conditions for bremsstrahlung rejections.

2.3.2 Bremsstrahlung Rejection.

The germanium detector is centrally placed in the detection set up with the four quadrants of the sodium iodide detectors surrounding it. Two of the quadrants of the NaI(Tl) counters detect the oppositely directed annihilation quanta, 511 keV in coincidence, the other two quadrants are used to detect bremsstrahlung radiation. The bremsstrahlung rejection was achieved by rejecting any pulse from germanium if an event in the other pair of quadrants corresponding to an energy transfer of 50 keV or more, was detected.

2.4 ELECTRONIC CIRCUITRY

The output from the charge-sensitive preamplifier of the central detector is amplified and gated by the

output of the annulus coincidence circuitry which responds to an appropriate coincidence amongst the quadrants, within a resolving time. The set condition is such that an event is acceptable if 511 keV photopeaks are detected from one pair of diametrically opposite quadrants, but no pulse height corresponding to energies greater than 50 keV is detected from either members of the other pair of quadrants, and a pulse is generated at the output of the three-input AND gate. The two AND gates are then connected to an OR gate and linearly gated to the signal from the central detector. A detailed illustration of the electronics circuitry is shown in Fig. 2.10.

Linear signals from the central detector are then selected for analysis. The pulses were digitized by a 50 MHz ADC and acquired in an 8000 channel analyser based on a Nova 2 minicomputer. The system was stabilized by fixing the channels of one of the peaks.

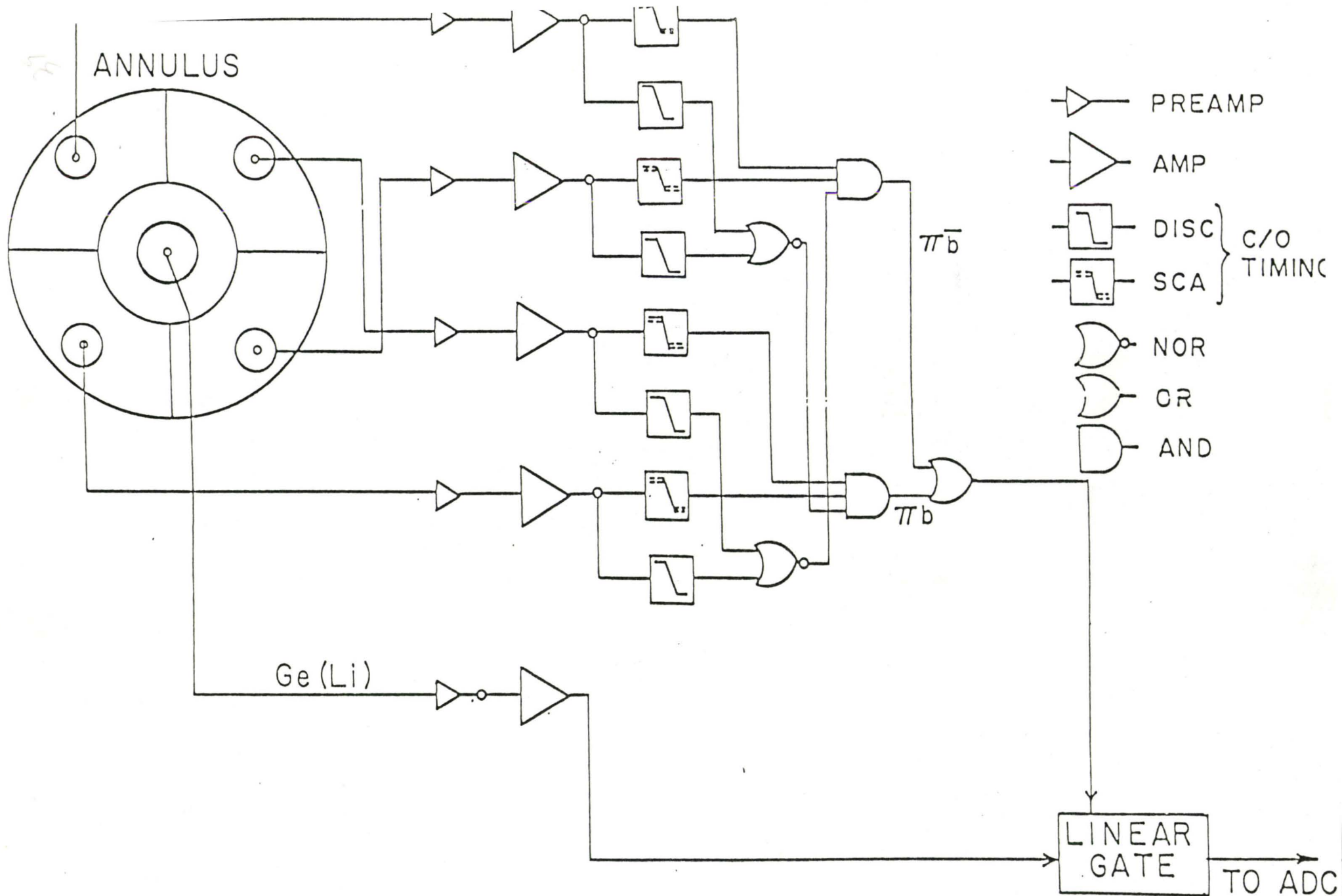


Figure 2.10 ELECTRONIC CIRCUITRY

CHAPTER 3

EXPERIMENT

3.1 THEORY

3.1.1 Energy

In the measurement of energies of capture gamma rays many different techniques have been employed. The most frequently used among them are the 'Bootstrapping' method, the use of cascade cross-over relationship and the mass-energy conversion method.

The idea of bootstrapping is based on the knowledge of the spacing between the three peaks due to single- and double-escape peaks and the full energy peak. In the output pulse height spectrum, the spacings are equal and precisely proportional to 511.006 keV. In the germanium detector, there is the production of positron-electron pair. When one or both escape and they are not detected, the corresponding peaks are referred to as single- and double-escape peaks respectively. When the two are detected, that is, no escape, the peak is said to be a full energy peak. For example, it is possible to determine the energy of the double-escape peak due to a

6 MeV γ -ray relative to the nearby full energy peak, due to a 5 MeV γ -ray which is well known. First the small energy separation is measured and it is used to determine the energy of the double-escape peak. Then 1022.01 keV is added to this energy to obtain the actual energy of the 6 MeV γ -ray.

The advantage is that errors due to the nonlinearities, calibration errors in detecting and analysing systems, do not come to play particularly when the energy separation determined is very small. Error may be considerably high when using peaks which are widely spaced.

The common problem encountered when the bootstrapping method is used, is the shifting of the full-energy peak. This occurs when biasing an electric field in a planar detector.⁽²⁶⁾ This electric field accelerates or decelerates the secondary electrons produced by γ -rays, depending on the direction the electrons were moving with respect to the field. Photoelectrons, for example, could be accelerated adding energy to a photo peak whereas the net effect on positron-electron pairs, moving roughly

parallel to each other would be to leave a pair-escape unshifted since the acceleration of the electron would be compensated by the deceleration of the positron. This peak shifting effect has been drastically reduced since co-axial geometry detectors have been constructed.

Another method commonly used in energy gamma rays measurement is the cascade cross-over relationship which employs branching of the decay of excited states through an intermediate level. To obtain the energy of the excited states, the energies of the two cascade gamma rays should be known with high precision. Both energies lie in the low energy region in order that, when summed up, they will give the energy of the excited state and hence the ground state transition energy. Suitable correction must be made with each of the gamma ray emission for the small recoil energy associated with them.

Mass difference between the target nucleus and the resulting ground state due to thermal neutron capture, is another method sometimes used in the determination of the energy γ -rays. The energy a gamma ray has can be

calculated from the accurately known masses of the initial and final states of the system and by using the mass-energy conversion factor.⁽²⁷⁾ Greenwood and Helmer⁽²⁸⁾ established the γ -ray energies and ^{15}N excitation energies between 5.27 MeV and 9.16 MeV with accuracies of 0.10-0.22 keV, by making a least-squares fit to the positions of the various peaks due to cascade γ -rays and using a neutron binding energy value of (10883.64 ± 0.13) keV. The mass energy conversion factor is 931.4812 ± 0.0052 MeV/u. This value is quoted from a report by Taylor et al.⁽²⁹⁾

In this present work the experiments were carried out with the pair spectrometer, so only the peaks corresponding to the double escape were obtained. An automatic peak extraction technique was employed. The square root of the original spectrum was taken so that the standard deviation associated with the contents of each channel will be $\sigma_{sq} = 0.5$.⁽³⁰⁾ The spectrum was filtered by convolving the resultant data with a zero area rectangular correlator to enhance the signal-to-noise ratio by a factor of about four. Figure 3.1 shows the original spectrum, zero area filter and the convolved spectrum. The variance σ_c^2 introduced into each point in the correlation spectrum

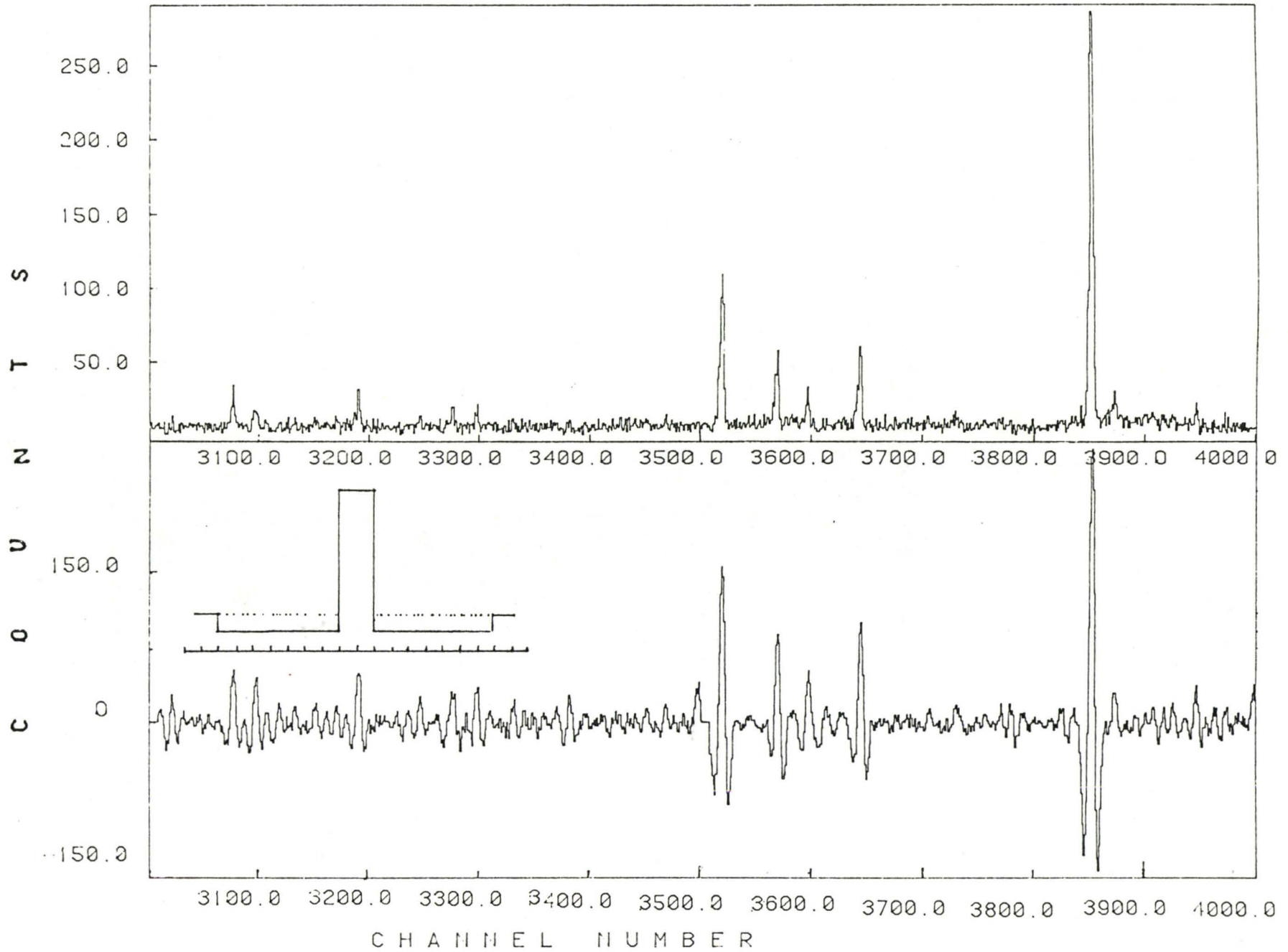


Figure 3.1 shows original spectrum, zero area digital filter and convolved spectrum.

was calculated and the detection of signal content was obtained by setting an appropriate $3.4873 \sigma_c$ discrimination level in the correlation spectrum. The centroids of the peaks were determined using positive points in the convolution data.

The centroids of the peaks of well known lines of nitrogen were used for the calibration applying a least square fit. The effect of non-linearity, due to the peaks which were fairly widely spaced, was taken care of by assuming a linear relationship between pulse height and energy, and gain obtained from this was plotted as a function of energy.⁽³¹⁾ The data points used define the trend of the non-linearity function but, because of associated errors in the reported energies, considerable dispersion prevailed. The transform function was obtained by constructing a smooth slowly varying curve which followed the general pattern exhibited by the data points. The shape of the transformation function is shown in Figure 3.2. The maximum deviation from linearity was 1.06 keV for the energy range (2.5 MeV - 7.3 MeV) considered.

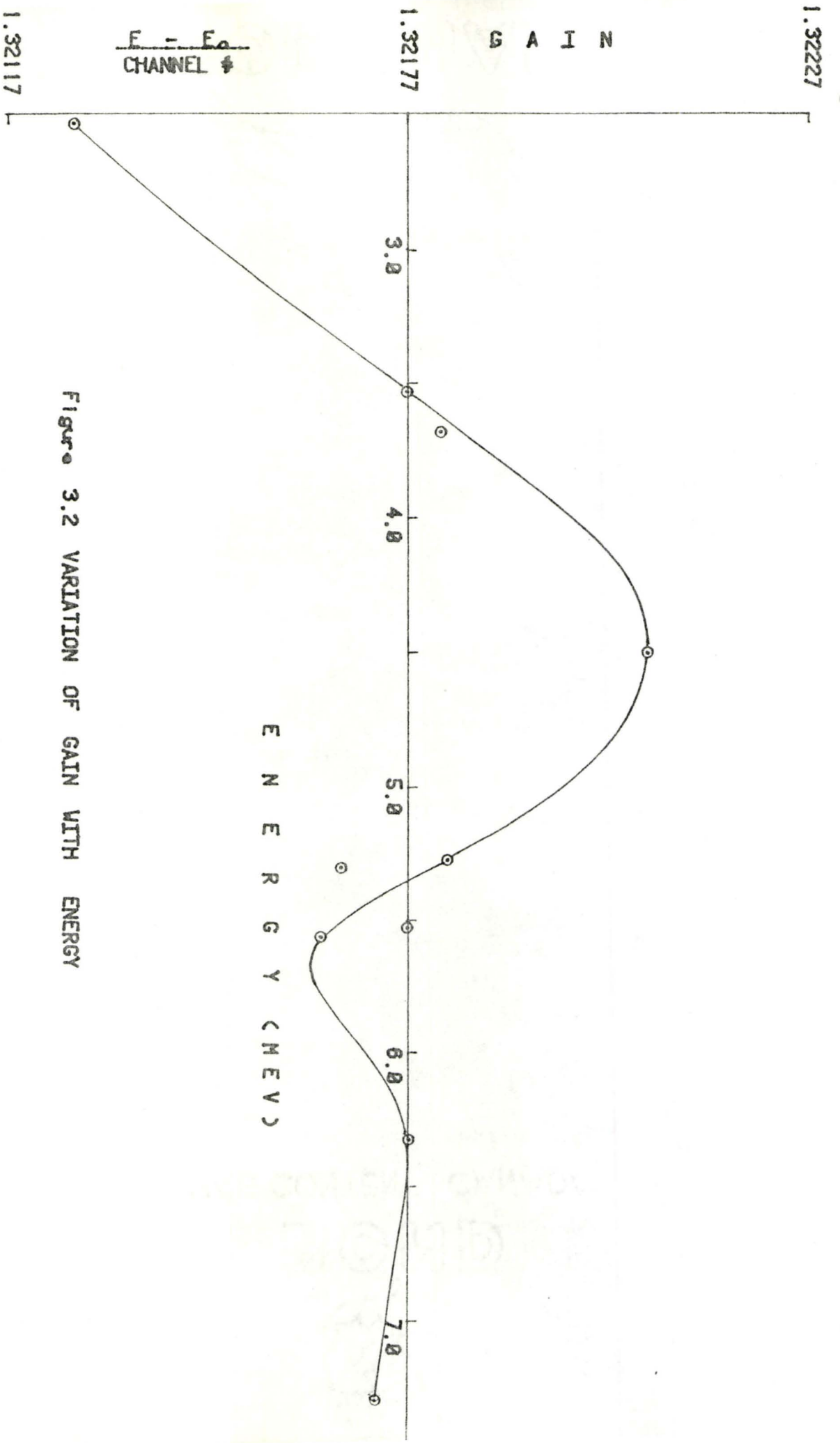


Figure 3.2 VARIATION OF GAIN WITH ENERGY

The maximum uncertainty in the γ -ray energy of known Nitrogen lines was added to the error in determination of the mean of the Gaussian energy peak. This was taken as the error in the energy of each gamma ray.

3.1.2 Intensity.

The intensities of the transitions were determined by first measuring the area of each peak. The method of maximum area technique was used. The gross area minus the continuum in the background gives the actual required peak area. This continuum was estimated from the adjacent regions assuming a linear variation, that is, as seen from Figure 3.3

$$S = \sum_{i=i_1}^{i_2} S_i - \sum_{j=j_1}^{i_1-1} S_j - \sum_{k=i_2+1}^{i_2+(i_2+i_1-1)/2} S_k$$

where S_i constitutes the gross area. S_j and S_k are the continuum and their subscripts refer to channel numbers. This was moved across the peak to obtain maximum area. The total areas contributed by the observed ^{58}Fe peaks due to primary transitions were also obtained.

The relative intensity of each transition is

$$I_A = \frac{N_A}{N}$$

where N_A is the area of a particular peak A and N the total

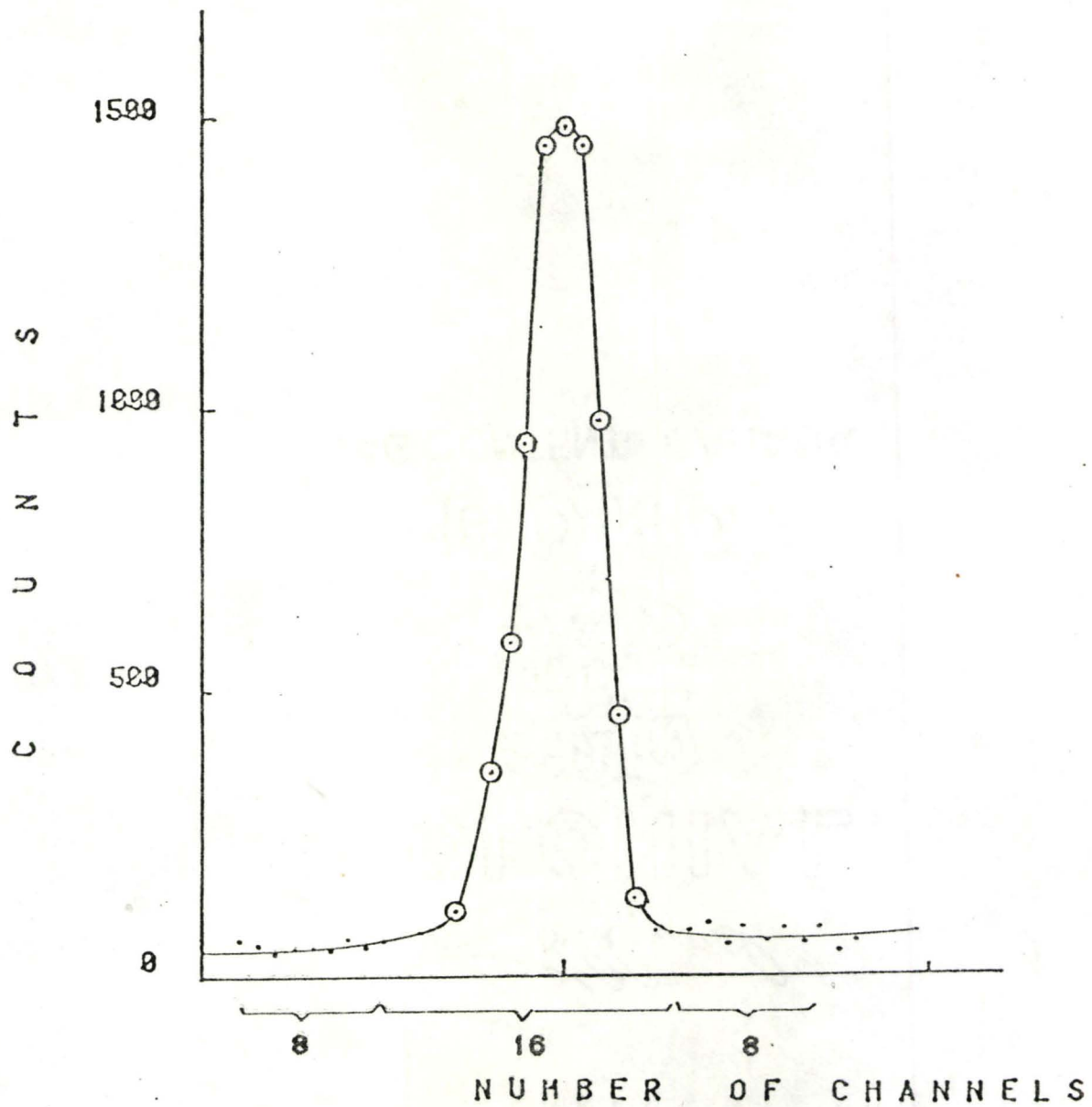


Figure 3.3 ILLUSTRATION OF PEAK AREA DETERMINATION

area contributed by all peaks due to primary transitions observed in ^{58}Fe . N_A and N have been corrected for the detector efficiency. The detector efficiency is obtained from a graph, see Figure 3.4. The efficiency is plotted as a function of energy gamma rays and was determined for each point used in the graph. By calculating the area of each peak of the known Nitrogen lines, and dividing by their well known intensities, the efficiency is obtained.

The error calculation was carried out by splitting total N counts to N_A and N_B , i.e.

$$I_A = \frac{N_A}{N_A + N_B} \quad \text{where } N = N_A + N_B$$

$$I_A = f(N_A, N_B)$$

I_A is intensity due to peak A

N_A is the number of counts in area under the peak A

N_B is total counts of all the areas under the peaks of ^{58}Fe minus N_A .

Since N_A and N_B are independent of one another $\sigma_{I_A}^2$ can be defined as

$$\sigma_{I_A}^2 = \left(\frac{\partial I_A}{\partial N_A} \right)^2 \sigma_{N_A}^2 + \left(\frac{\partial I_A}{\partial N_B} \right)^2 \sigma_{N_B}^2$$

E F F I C I E N C Y (P E A K A R E A / I N T E N S I T Y O F N I T R O G E N)

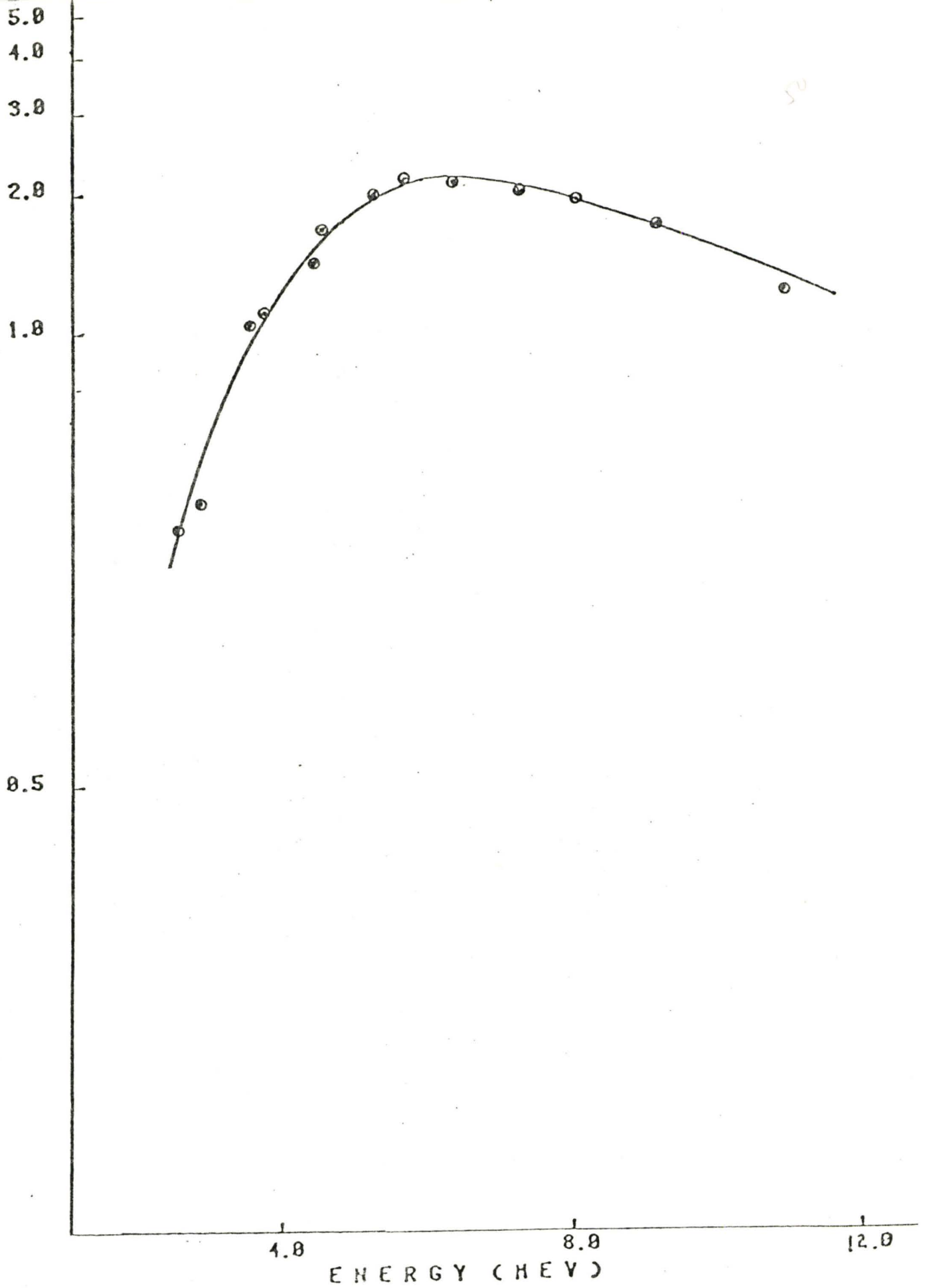


Figure 3.4 DETECTOR EFFICIENCY CURVE.

$$\sigma_{I_A}^2 = I_A^2 \left[\frac{1}{N_A} - \frac{1}{N} \right]$$

$$\sigma_{I_A} = I_A \left[\frac{1}{N_A} - \frac{1}{N} \right]^{1/2}$$

from this final relation one can say that the error in the intensity depends on intensity of that particular line I_A , peak area N_A and total peak areas of primary transition due to ^{58}Fe .

3.2 PROCEDURE.

A natural iron sample in oxide form, Fe_2O_3 , was first irradiated. The sample was in a powdered form and weighed about 1 gm. It was poured in a graphite capsule with a graphite top. The capsule was in turn attached to aluminum chains and nylon thread and then lowered into the irradiation position. It was irradiated for several hours. While irradiating a pump was used to evacuate air and nitrogen from the through tube, and kept constantly at low pressure.

The iron isotope ^{58}Fe sample used was also an oxide, Fe_2O_3 , in a powdered form. The sample weighed 13.4 mg containing 10 mg of the enriched iron isotope ^{58}Fe .

This tiny powder sample was carefully poured to the bottom of a small beryllium capsule which has been specially designed for irradiation of small-quantity samples. The sample, in the small beryllium capsule, was covered with aluminum foil to prevent particles falling from the graphite top and mixing with the sample. It was irradiated for several days. The spectrum obtained were carefully watched to ensure that there was no drifting or shifting of the peaks. The data was taken daily in order to check for any development that might arise day after day, and was stored on magnetic tape.

Nitrogen has lines which are well spaced over the range of energy gamma rays under consideration. These lines are also well known. For the calibration purposes, there was a mixed experiment of nitrogen gas plus the sample ^{58}Fe . The irradiation tube was flooded with nitrogen gas at a high pressure a little above atmosphere, to increase the counting rate. This mixed sample was irradiated for several hours.

The irradiation of the natural iron sample was repeated for another few hours. This was to make sure that the detection system was in good condition throughout

the experiment.

The isotope ^{58}Fe sample used was in a beryllium capsule. One expects that beryllium lines will be present in the spectra. To take care of any contribution due to the impurities in the capsule, an empty and clean beryllium capsule was irradiated for several hours. The spectrum obtained from this experiment and all other spectra, were used for analyzing the data. Table 2 is a summary of the irradiation time, samples and materials used. Figures 3.5 - 3.8 are spectra obtained from the experiments.

TABLE 2

SUMMARY OF SAMPLES, MATERIALS AND IRRADIATION TIME				
Sample	Mass	Physical form	Hours of run	Capsule used as container
Natural iron	1 gm	Powder	50	C
^{58}Fe	10 mg	Powder	78	Be
^{58}Fe singles	10 mg	Powder	22	Be
^{58}Fe	10 mg	Powder	58	Be
^{58}Fe +nitrogen	10 mg + atom. Pressure	Powder+ gaseous	20	Be
Natural Iron	1 gm	Powder	10	C
Empty Be capsule	4 gm	Solid	24	Be

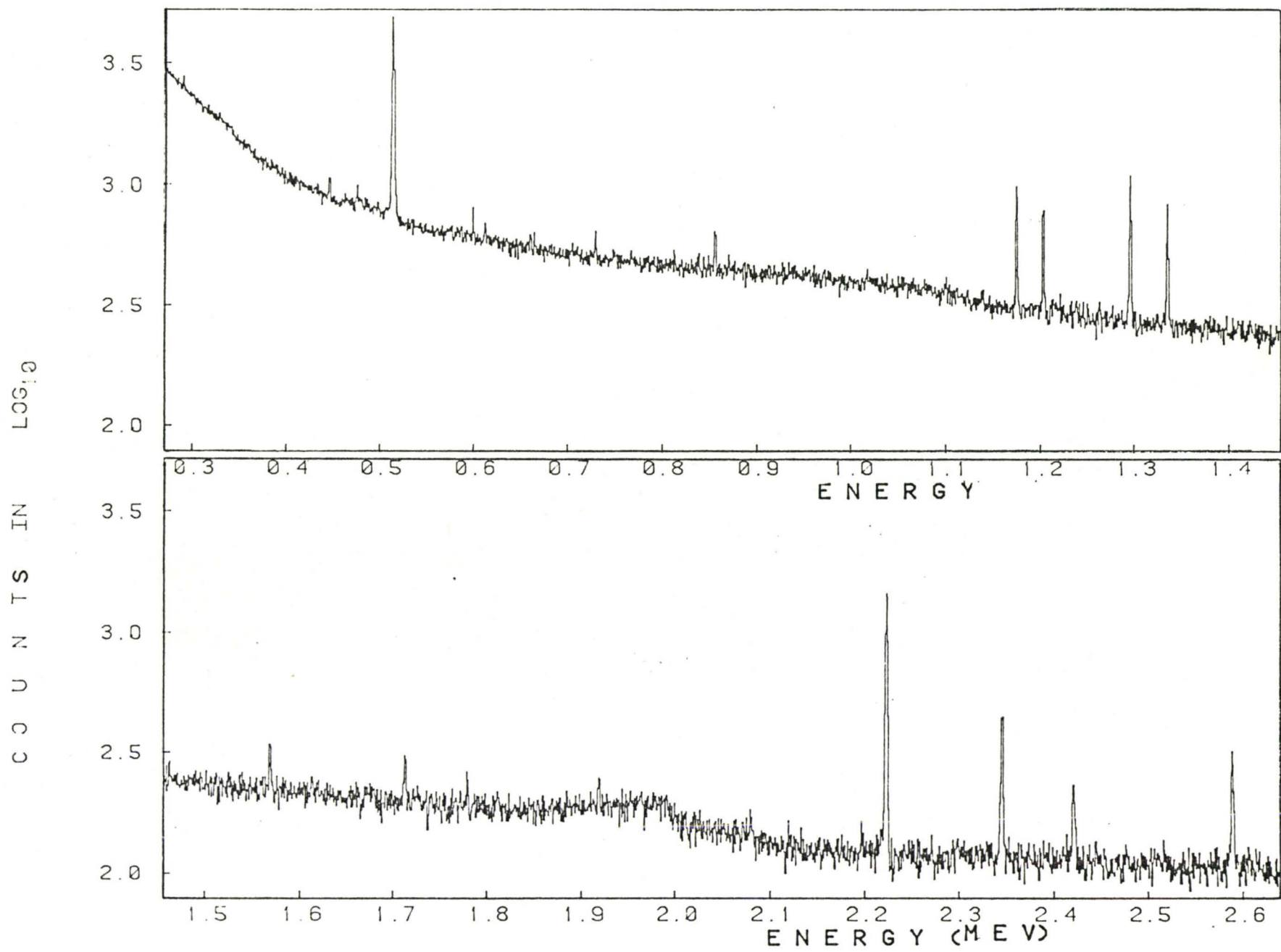


Figure 3.5a SPECTRUM OF IRON ISOTOPE (FE58) IN SINGLES MODE (Part 1)

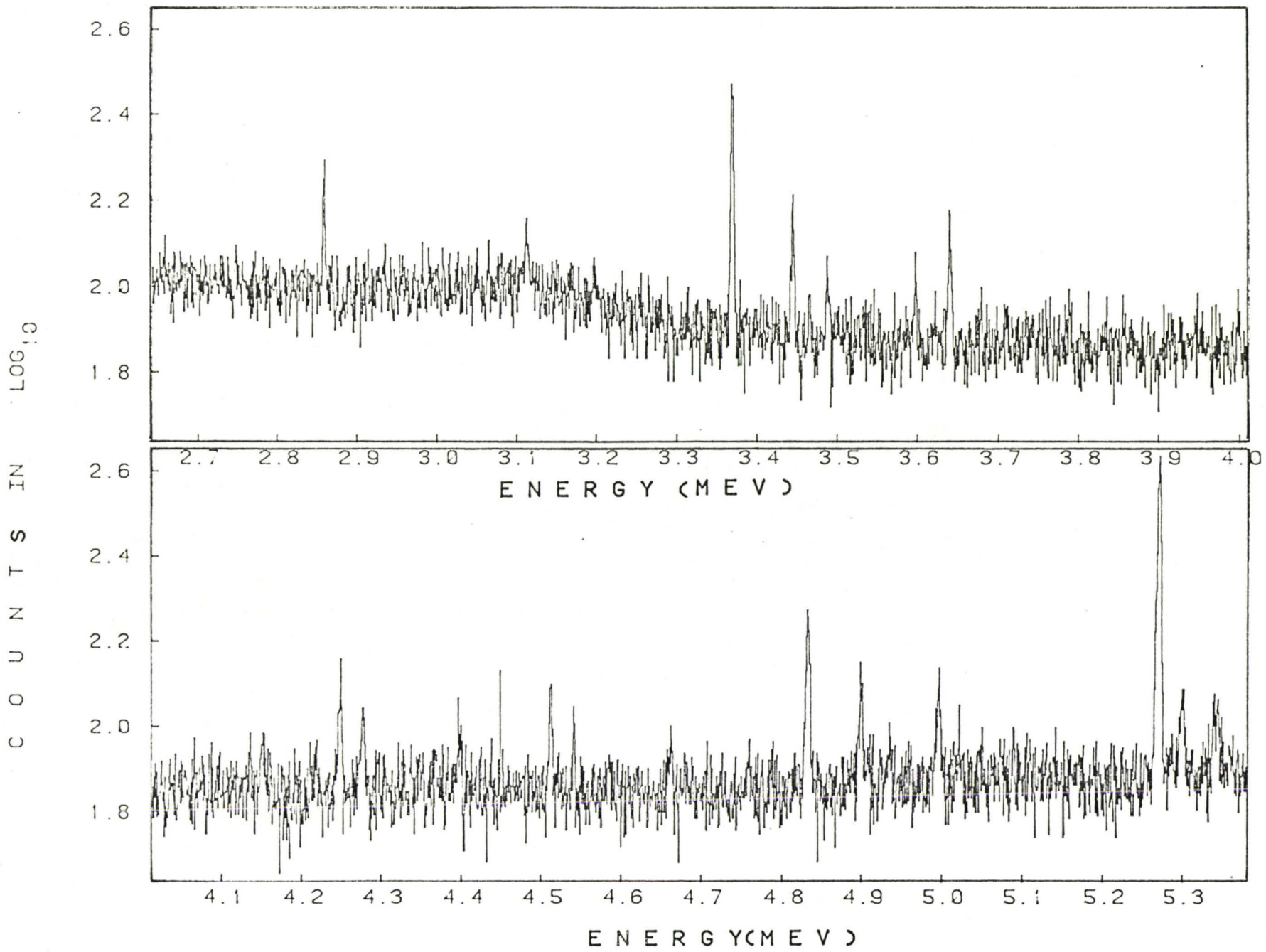


Figure 3.5b SPECTRUM OF IRON ISOTOPE (FE58) IN SINGLES MODE (Part 2)

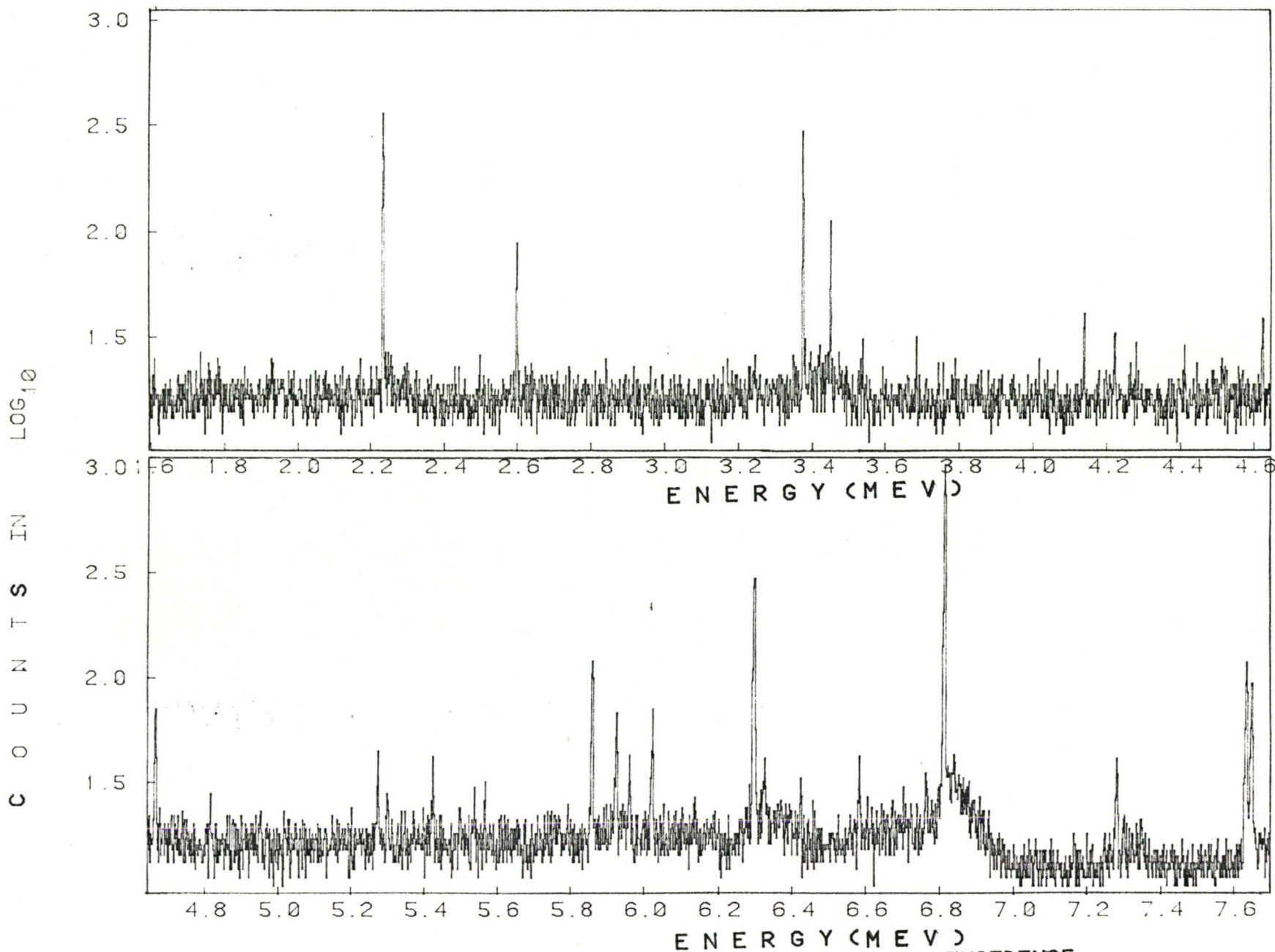


Figure 3.6 SPECTRUM OF IRON ISOTOPE (FE58) IN TRIPLE COINCIDENCE

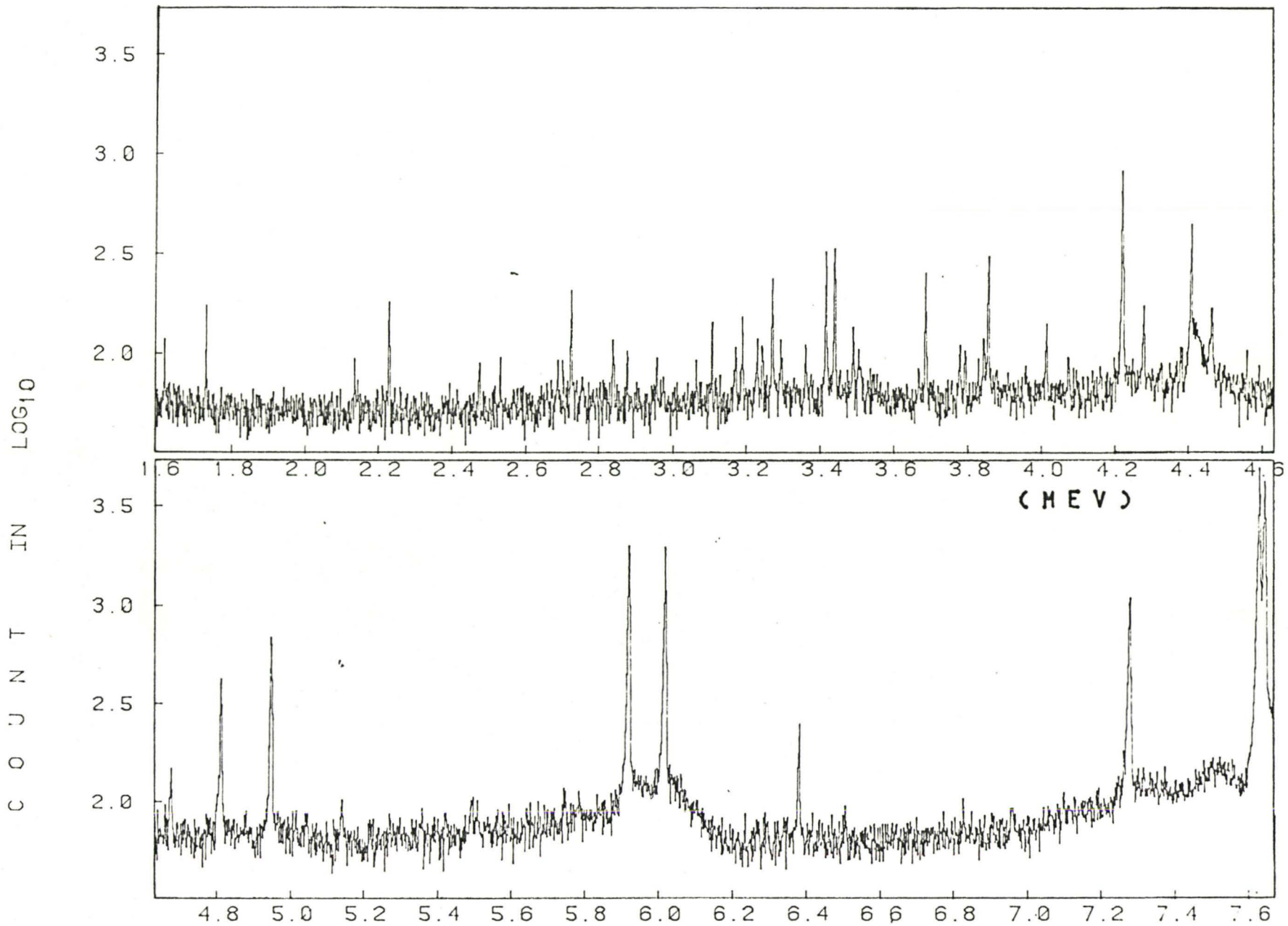


Figure 3.7 SPECTRUM OF NATURAL IRON IN TRIPLE COINCIDENCE (MEV)

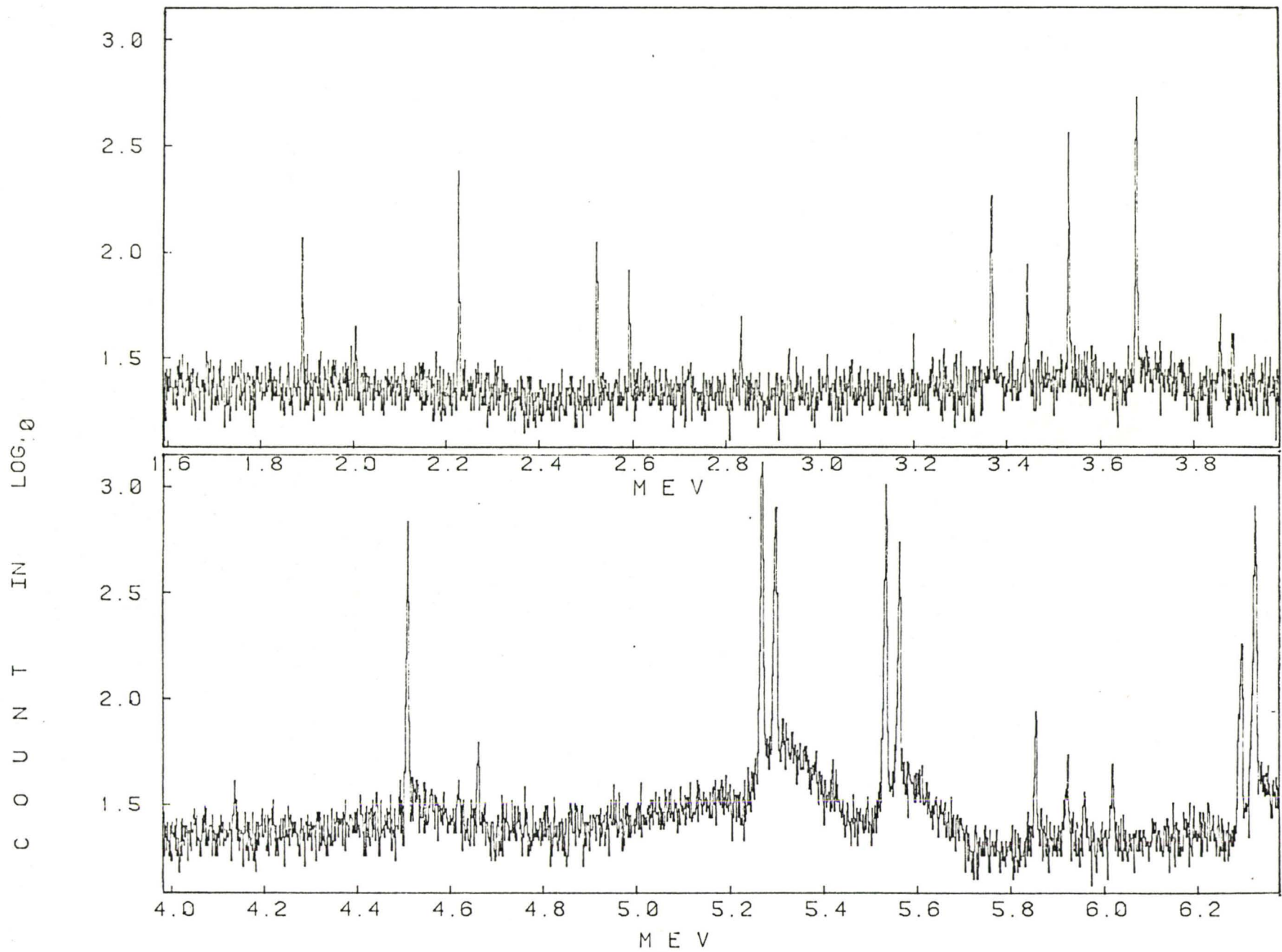


Figure 3.8 SPECTRUM OF NITROGEN AND ⁵⁸FE IN TRIPLE COINCIDENCE

CHAPTER 4

DATA ANALYSIS

The experimental set up was such that the system operates as a triple coincidence pair spectrometer at high energies. At low energy the triple coincidence is removed and the system is operated at singles mode.

4.1 Gamma Ray Energy

In the determination of the energy of a spectral peak, three main points were considered to ensure that the energy is as accurate as possible. One is the location of the exact peak centre which is highly essential. To attain this, an automatic peak extraction technique was used. This requires the convolution of the spectrum with a zero area filter which mathematically, is analogous to second differentiation.⁽³²⁾ The peak, which is a form of a Gaussian distribution, is transformed into a central peak with satellite negative lobes. The peak centroid is obtained by finding the mean of the central positive lobe. The centroid obtained by this method is used as the peak centre. This method was applied to all the peaks used in the analysis; they are the strong

beryllium lines Be(2589.9), Be(3368.2), Be(3444.4) and Be(6810.0) together with the strong lines of nitrogen, N(2521.06), N(3532.22), N(3677.61), N(4507.68), N(5269.03), N(5298.11), N(5533.38), N(5562.46), N(6322.48) and N(7299.27). This method was used for all the observed lines of the iron isotope ^{58}Fe .

Another important issue in the determination of energy of a spectral peak is the instrument non-linearity. The electronic set up does not yield a linear relation between the energy and peak centre. The step taken to correct the non-linearity of the system was by assuming a linear relationship between pulse height and energy, plot the deviation as a function of energy and obtain corrected gain for each energy from the slowly varying curve.

The third step is the consideration of the lines used for the calibration. In the determination of centroids of peaks, beryllium and nitrogen lines, mentioned above, were carefully considered. These lines were used because they are intense and well known. Beryllium lines were present in the spectrum because of the capsule used. Nitrogen lines were also used because

a mixed run of ^{58}Fe and nitrogen was carried out so the energies of the peak centres were determined, using the intense lines of well known energies which were present in the spectrum.

TABLE 3

Energies and intensities of γ -rays from the primary transitions of reaction $^{58}\text{Fe}(n,\gamma)^{59}\text{Fe}$

Thermal (n, γ) Reaction Measurements by A.P. Bogdanov		Resonance (n, γ) Reaction Measurements by J.C. Wells, Jr.		PRESENT WORK Neutron Capture Gamma Reaction $^{58}\text{Fe}(n,\gamma)^{59}\text{Fe}$			
E_γ (± 3 to 6 keV)	I_γ	E_γ keV		E_γ			I_γ
4137	4.2	4133.5	3.0	4135.55	0.20	6.00	0.36
4618	4.2	-	-	4620.95	0.22	4.23	0.31
4660	9.1	4661.6	3.0	4663.23	0.19	12.58	0.51
5420	2.5	5418.7	2.0	5419.60	0.25	3.88	0.30
5854	16.8	5854.7	3.0	5855.53	0.18	17.95	0.51
-	-	6010.4	3.0	6011.18	0.30	1.97	0.51
6295	51.0	6294.5	2.0	6294.70	0.13	52.62	0.77
6582	2.3	6580.5	3.0	6581.53	0.26	2.74	0.25

Two different experiments of the iron isotope ^{58}Fe alone were carried out. The data obtained from these experiments were treated separately to determine the energies of the principal components. In the triple coincidence mode **eight** primary lines of ^{58}Fe were observed. Their energies were determined separately in each of these experiments. The final energy gamma rays listed in Table 3 are a result of the mean values or weighted average values of each line.

The low energy gamma rays were determined from the spectrum obtained in the singles mode. The known lines of ^{12}C , ^{41}Ar and ^{60}Co that appear in the spectrum as impurities were also used in low energies of the singles mode. The energies obtained from this single mode spectrum are the low energies that can not be detected with the triple coincidence pair spectrometer, and they correspond to secondary transitions. They form the cascades together with the primary transitions. Their values are listed in Table 4.

The uncertainties in the energy of the gamma rays are obtained from the summation of two errors. The first one is the **error associated with**

TABLE 4

Secondary γ -rays from the $^{58}\text{Fe}(n,\gamma)^{59}\text{Fe}$ reaction

Thermal (n, γ) Measurement*		Resonance (n, γ) Measurement**		Neutron Capture Gamma $^{58}\text{Fe}(n,\gamma)^{59}\text{Fe}$ Reaction - Measurement	
E_{γ}	I_{γ}	E_{γ}		E_{γ}	I_{γ}
287	58.0	287.8		287.71	0.30
-	-	472.6		473.22	0.50
728	18.0	725.8		726.94	0.35
1162	1.6	1162.8		1162.80	0.50
1922	7.3	1917.3		1918.59	0.30

* Values were taken from report by A.P. Bogdanov et al.⁽⁷⁾ The gamma ray energies have accuracies of $\pm 3-6$ keV.

** The gamma ray energies were quoted from a report by J.C. Wells, Jr. et al.⁽¹⁰⁾ with accuracies of $\pm 0.9 - 1.5$ keV.

the determination of the mean, peak centre. This is determined by first assuming that the peak is Gaussian, that is, it is a bell-shaped curve symmetric about the mean, μ . The width of the curve is characterized by a full-width at half-maximum (FWHM), which is generally called the half-width Γ . This is defined as the range of x between the values at which the

Gaussian probability distribution function $p_G(x, \mu, \sigma)$ is half its maximum value⁽³³⁾

$$p_G(\mu \pm \frac{1}{2} \Gamma, \mu, \sigma) = \frac{1}{2} p_G(\mu, \mu, \sigma), \Gamma = 2.354\sigma .$$

Since the first step in the determination of the energy of a spectral peak, is the determination of the mean, this error was taken as one of the errors. In calculating the error in the energy of the peak, the half-width was first determined and standard deviation was obtained in every peak.

The other error was due to non-linearity and the assumed well-known lines. Fit was made using known gamma ray energies obtained from Dr. Kennett.⁽³¹⁾ The error associated with the gamma ray energies used is of the order of one-tenth of keV. To obtain the final error in the energy of a spectral peak it was assumed that the errors add, so the standard deviation was added to the maximum error in the γ -ray energies used. This means that the errors have been maximized.

As already stated, two different experiments were considered separately and the mean or weighted average taken. The weighted errors were also considered for the final error.

Figure 4.1 is the proposed decay scheme of ^{58}Fe . Spin-parity assignments are from J.C. Wells, Jr. (10) and Nucl. Data Sheet. (34)

TABLE 5
Determination of Neutron Separation Energy

	6581.92	6581.92
287.71	6295.06	6582.77
726.94	5855.84	6582.78
1162.81	5419.87	6582.68
1918.62	4663.43	6582.05
	mean	6582.44 \pm 0.42

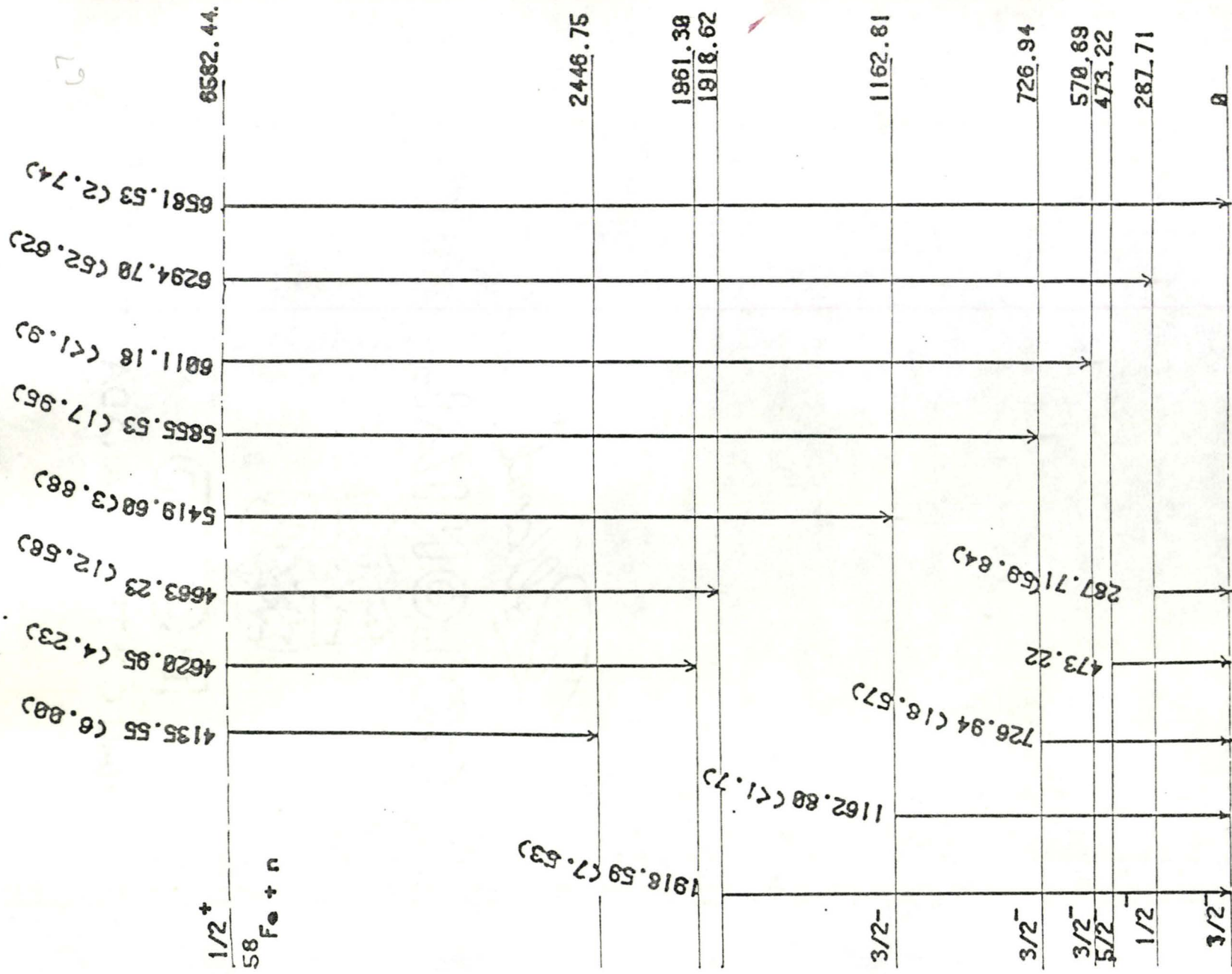


Figure 4.1 DECAY SCHEME OF ^{59}Fe

4.2 Neutron Separation Energy.

In the determination of neutron separation energy four of the sets of cascades were used together with the transition to the ground state. A correction was added to the gamma ray energies due to nuclear recoil, as given by the formula⁽¹¹⁾

$$\Delta E(\text{keV}) = \frac{0.537 \times [E_{\gamma}(\text{MeV})]^2}{A} .$$

The values obtained are listed in Table 5. The final value of the neutron separation energy was obtained using the weighted average of the values. The mean, or weighted average is 6582.44 ± 0.42 keV.

4.3 Intensity Determination.

In the determination of the intensities of the lines as stated in Table 3, two main steps were taken. First the intensity of the primary lines were determined. The peak areas of all the lines were calculated using the maximum peak area method. Each peak corresponds to a particular energy and the detector efficiency factor for each of the peaks was obtained from the graph (Figure 3.4). This was used to divide each peak counts. The resulting peak

areas were added and used to determine the relative intensity of the primary lines

$$I_A = \frac{N_A}{N}$$

and the error associated with each line intensity was determined and listed in Table 4. This is given as

$$\sigma_{I_A} = I_A \left[\frac{1}{N_A} - \frac{1}{N} \right]^{1/2} .$$

The intensities of the secondary lines were calculated using the intensity values obtained from A.P. Bogdanov⁽⁷⁾ and the relative values calculated for the primary transitions. The intensities of the secondary lines are also listed in Table 4.

As a check on the intensity values another line of action was taken. The intensity of the most intense lines was determined from the ratio of yields of that peak of ^{58}Fe (6294.70keV) and ^{56}Fe doublet peaks. The relationships used are

$$Y_{58} = n_{58} \sigma_{58} I_{58} \epsilon(E_{58})$$

and

$$Y_{56} = n_{56} \sigma_{56} I_{56} \epsilon(E_{56}) .$$

Y_{58} is the yield, the area of peak (6294.70) of ^{58}Fe ,
 n_{58} is the number of nuclei of ^{58}Fe present in the
sample, σ_{58} is the capture cross section of ^{58}Fe ,
 I_{58} is the intensity of the line (6294.70 keV) of ^{58}Fe
and $\epsilon(E_{58})$ is the detector efficiency at that particular
line (6294.70 keV) of ^{58}Fe . Y_{56} , n_{56} , σ_{56} , I_{56} and $\epsilon(E_{56})$
are the corresponding values of the doublet peaks
(7631.6; 7645.6 keV) of ^{56}Fe .

The peak area of (6294.70 keV), Y_{58} and the peak
area of Y_{56} of the doublet (7631.6; 7645.6 keV) of ^{56}Fe
were determined from the same experiment. It was discovered
that there was some contribution to the peak area of the
doublet from the iron present in the capsule. To correct
for this a separate experiment of the empty beryllium
capsule was carried out. From the spectrum obtained, the
peak area of the beryllium line Be(6810.0 keV) was
deduced and the iron doublet (7631.6 - 7645.6 keV) peak
area was also deduced.

	Peak Area
Be(6810.0)	103,465
^{56}Fe (doublet) (7631.6 - 7645.6)	4,459 .

This gives a ratio $^{56}\text{Fe}/\text{Be}$ of 0.0431. For the run involving ^{58}Fe only three peak areas were taken. They are

	Peak Area
$^{58}\text{Fe}(6293.2 \text{ keV})$	4,911
$\text{Be}(6810.0 \text{ keV})$	12,753
^{56}Fe (double) (7631.5 - 7645.6 keV)	3,638 .

The contribution to doublet peak area from the capsule is $0.0431 \times 12753 = 550$. This reduced the yield Y_{56} to $3638 - 550$, therefore, $Y_{58} = 4911$ and $Y_{56} = 3088$. The value of n_{58} and n_{56} used are 76.54 and 20.99 as listed in Table 1. These values were quoted from the values of composition of the sample of enriched ^{58}Fe , from Oak Ridge, and they were used because only the ratio of the two values is necessary in the calculation. The values of the capture cross section were obtained from S.F. Mughabghab and D.I. Garber, ⁽⁴⁾ $\sigma_{58} = 1.15 \pm 0.02 \text{ b}$ and $\sigma_{56} = 2.63 \pm 0.21 \text{ b}$. The doublet combined intensity

$I_{56} = 52.1 \pm 1\%$ was quoted from M.L. Stelts and R.E. Chrien.⁽³⁵⁾ The detector efficiencies at the two energies are $\epsilon(E_{58}) = 2.2$ and $\epsilon(E_{56}) = 2.0$. For example

$$\frac{4911}{3088} = \frac{76.54}{20.99} \times \frac{1.15}{2.63} \times \frac{I_{58}}{53.1} \times \frac{2.2}{2.0}$$

and $I_{58} = 47 \pm 5$. The percentage error when estimated is shown to be greater than 10%. If this is taken into consideration intensity values will agree.

CHAPTER 5

DISCUSSION OF RESULTS

Eight primary transitions were observed. The energies of the gamma rays corresponding to these transitions were determined and the values are listed in Table 3. These values agree well with the values obtained from different reactions previously carried out by different groups. The values were in better agreement with one of the most recently published papers by J.C. Wells, Jr. et al.⁽¹⁰⁾ than the other values previously published. There is overlapping in all the values when the estimated error associated with each gamma ray is considered. The 4620.95 keV that was not detected by J.C. Wells, Jr. and his group⁽¹⁰⁾ was identified and measured accurately. Also the 473.22 keV and 6011.18 keV γ -rays which were not given any serious consideration in the thermal reaction work previously carried out by A.P. Bogdanov⁽⁷⁾, were also observed and the energies determined. 473.22 keV is one of the low-lying energy gamma rays detected and among the secondary lines that were detected are 287.71 keV, 726.94 keV, 1162.80 keV and

1918.59 keV as listed in Table 4. The estimated errors involved in the determination of the energies of these gamma rays are also listed in the Tables. A look at the estimated errors shows that the energies of the gamma rays are determined to a high degree of accuracy. Listed along with these values, on the Tables for comparison, are values previously published and obtained from different reactions.

The accurate energy gamma rays obtained enables one to deduce the neutron separation energy. There were cascades and the gamma ray energies were corrected for nuclear recoil. The neutron separation energy was obtained by adding the two cascade energies and taking the weighted average of four resulting values, plus transition to the ground state. The neutron separation energy was found to be 6582.44 ± 0.42 keV. This value agrees not with the value recently published by J.C. Wells, Jr. et al.⁽¹⁰⁾ using resonance neutron capture but with the thermal (n, γ) reaction value reported by A.P. Bogdanov.⁽⁷⁾ The former reported a value of 6580.8 ± 1.0 keV while the latter has the value 6582 ± 3 keV in his report.

In this present work the relative intensities were measured and listed in Tables 3 and 4. The estimated errors were also listed with them in these Tables. These intensities are very close to that obtained from thermal reaction reported by A.P. Bogdanov et al.⁽⁷⁾. The only exceptions are 4135.55 and 4620.95 keV lines which were reported to have the same intensity but all the experiments carried out in this present work, show that the line 4135.55 keV is more intense than the line 4620.95 keV. Also in this work the intensity of line 4663.23 keV is more intense than it has been previously reported. The low values of the estimated error and fair agreement with previous work is an indication that these intensity values are quite reasonable and reliable. An attempt was made to determine the intensities, using the yield expression and the doublet peak of ^{56}Fe and there was a remarkable difference in the values. For a particular peak 6294.70 keV this method yielded a value of 48.15 compared to 52.62. If the per centage error of 15% which might be involved in the determination of the intensity in the formula is considered, the value 52.62 which agrees well with 51.0 from the previous work, will be acceptable.

If 52.62 is an acceptable value, then this method can be used to determine the ratio of capture cross sections of iron isotopes ^{56}Fe and ^{58}Fe

$$\frac{\sigma_{^{56}\text{Fe}}}{\sigma_{^{58}\text{Fe}}} = 2.69 \pm 0.16 .$$

This value assumes a percentage error of 1.4 for Y_{58} , 1.8 for Y_{56} , 1.5 for the detector efficiency ratio, and 1.5 for the nuclei ratio. This value is larger than the deduced value 2.29 ± 0.23 obtained by taking the ratio of the $\sigma_{^{58}\text{Fe}}$ and $\sigma_{^{56}\text{Fe}}$ published by S.F. Mughabghab and D.I. Garber. (4)

Correlation of the $^{58}\text{Fe}(n,\gamma)^{59}\text{Fe}$ reaction with the (d,p) reaction was investigated. It was observed that there is a distinct anti-correlation between the two reactions which is consistent with A.P. Bogdanov et al. (7)

Some experimental and theoretical work previously carried out has shown that there is the existence of rotational band level structure in ^{59}Fe . (5,8,36,37) Sood (36) attempted a theoretical description of the structure of ^{59}Fe using the then known levels and Nilsson-model. His proposed rotational band structure

shows the 728 keV level as a rotational band level of $1/2^- [310]$ Nilsson orbit of which 287 keV level is the intrinsic excitation of the same $1/2^- [310]$ Nilsson band. He noted that coriolis coupling did not contribute significantly to the levels in this nucleus. He also compared the pairs ^{58}Fe - ^{59}Fe and ^{184}W - ^{185}W since the latter have the corresponding band structure in the well-established deformed region. He found the quantity $\delta J_{\text{exp}}/J_{\text{rigid}}$ for the Fe pair to be 12% which agrees with 16% for the W pair.

Some years later 570 keV was identified and the assignment of $3/2^-$ to this level produced certain discrepancies with Sood's results. McLean et al.⁽⁵⁾ claimed that the 570 keV seems probable to be $1/2^- [310]$ band and that the 728 keV level is expected to be $3/2^- [301]$. Recent publications^(8,37) however, have shown that his claim may be wrong. Warburton et al.⁽⁸⁾ suggested a probable $5/2^-$ assignment for the 570 keV level, which is very doubtful. He also noted that the $\ell=1$ spectroscopic factor for the 570 keV level was found to be quite small, $(2J+1) = 0.017$ so that the angular distribution could have very well been influenced by second-order processes. Pardo et al.⁽³⁷⁾ also did not agree with McLean et al.⁽⁵⁾ He observed that

the 726.94 keV level has transition to the 287.71 keV level, while no transition to this state is observed from the 570 keV state. He expected that since E2 rates should be enhanced in intraband transitions then the second member ($J^\pi = 3/2^-$) of the $K = 1/2^-$ rotational band should have a transition to the $K = 1/2^-$ band. He then suggested that the 726.71 keV level is the $3/2^-$ member of the $K = 1/2^-$ rotational band. This suggestion is quite independent of spin $3/2^-$ or $5/2^-$ assigned to 570.71 keV level by different groups.

The data obtained from this work supports the idea that the ground state of ^{59}Fe , $J^\pi = 3/2^-$, is an intrinsic excitation identified as $3/2^- [312]$ Nilsson band and so also the 287.8 keV level with a spin and parity of $1/2^-$ as $1/2^- [310]$ band. This 287.71 keV level has a rotation excitation built on it at energy 726.94 keV level with $3/2^-$ identified as $1/2^- [310]$ Nilsson band.

Similar situations have been reported to exist in ^{179}Hf , ^{181}Hf and ^{183}W . A.I. Namenson et al. (38) observed in $^{178}\text{Hf}(n,\gamma)^{179}\text{Hf}$ and $^{180}\text{Hf}(n,\gamma)^{181}\text{Hf}$ reactions unusually strong E1 transitions proceeding from the capture state to the $1/2^-$ and $3/2^-$ levels of the $1/2^- [510]$ Nilsson band. The E1 transitions to the 287.8 keV and 726.94 keV

levels (in ^{59}Fe) of $1/2^-$ and $3/2^-$ respectively and identified as the $1/2^-$ [310] band are also unusually strong. Similarly intense transitions to the $1/2^-$ [510] Nilsson band were also observed, (39-41), in the ^{183}W isotope formed from thermal neutron capture reactions. Transition to a nearby $3/2^-$ member of the $3/2^-$ [512] Nilsson band (to which E1 transition is allowed) in a tungsten isotope, was relatively weak. In the same way the transition to the nearby $3/2^-$ member of the $3/2^-$ [312] in this work was relatively weak. The ratio (3:1) of the intensities of transitions in ^{59}Fe to the 287.71 keV $J^\pi = 1/2^-$ and 726.94 keV $J^\pi = 3/2^-$ levels of $1/2^-$ [310] band agree fairly well with the ratios (5.9:1 and 3.4:1) of intensities of transitions to the $1/2^-$ and $3/2^-$ levels in the $1/2^-$ [510] band in ^{179}Hf and ^{181}Hf respectively. Also the ratio of intensities of transition to the $1/2^-$ and $3/2^-$ level in the $1/2^-$ [510] band in ^{183}W is (4.3:1). Figure 5.1 shows the comparison of the intensities of the transition to the $\{1/2^-$ [310], $1/2^-$ [510]; $3/2^-$ [310], $3/2^-$ [510] and $3/2^-$ [312], $3/2^-$ [512]\} Nilsson bands.

Furthermore, Nilsson diagram shows that $1/2^-$ [510] band is a result of deformation of $f_{5/2}$ level just like

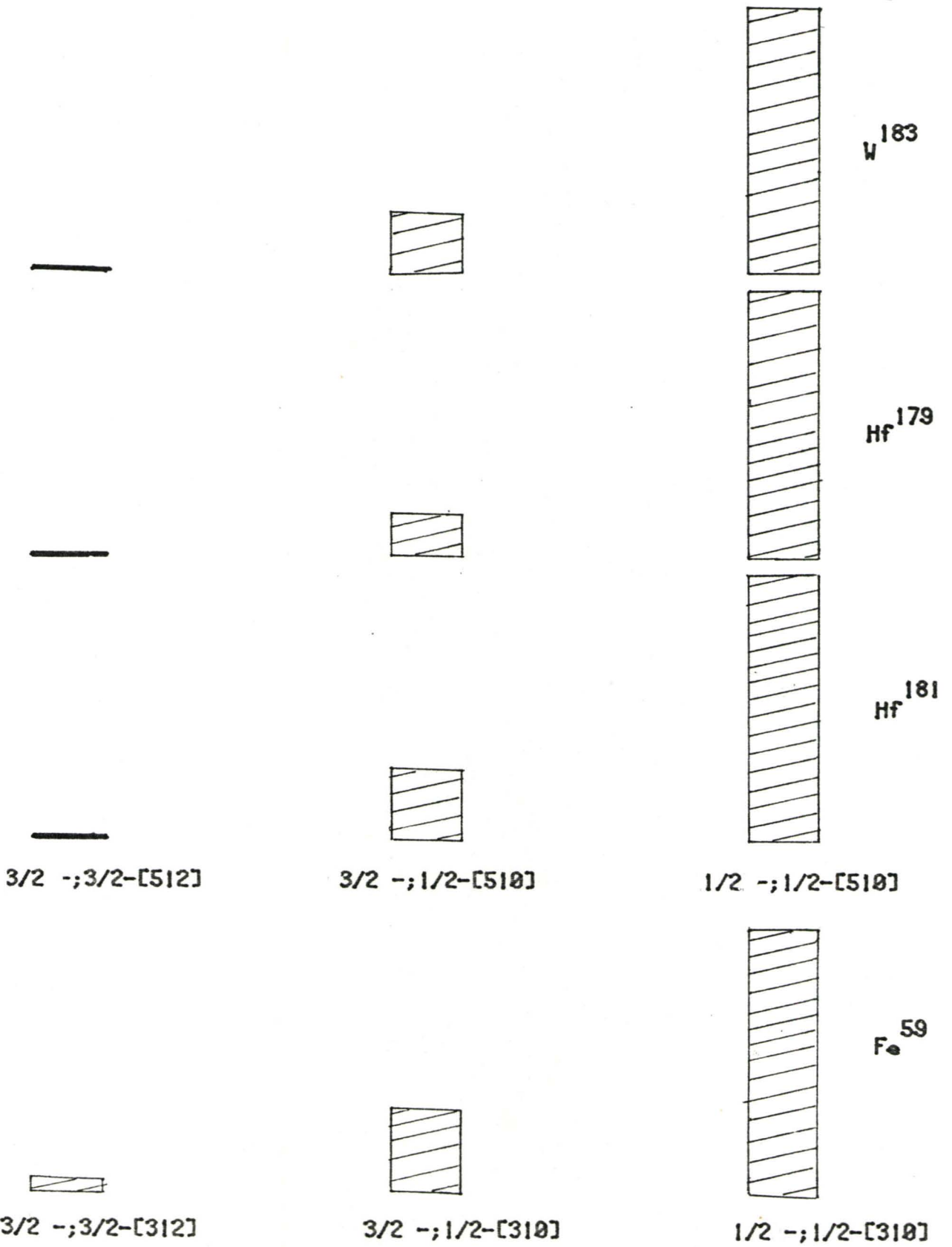


Figure 5.1 INTENSITY AGAINST NILSSON BAND

$1/2^-$ [310] is from $f5/2$ level. Similarly, the $3/2^-$ [312] is a result due to the deformation of $p3/2$ level just as $3/2^-$ [512] is. To be more convincing, the averages of intensities of transitions to $1/2^-$ [510], $3/2^-$ [510] and $3/2^-$ [512] Nilsson bands in Hf and tungsten isotopes were taken together. The value of the intensities of transitions in ^{59}Fe to $1/2^-$ [310], $3/2^-$ [510] and $3/2^-$ [512] Nilsson band were plotted against the values obtained from Hafnium and tungsten isotopes. Figure 5.2 shows the strong relationship between these sets of experimental data.

From this discussion, the author suggests that the 726.94 keV level of $3/2^-$ is a rotational excitation built on the 287.71 keV level of $1/2^-$ level both associated with $1/2^-$ [310] Nilsson band.

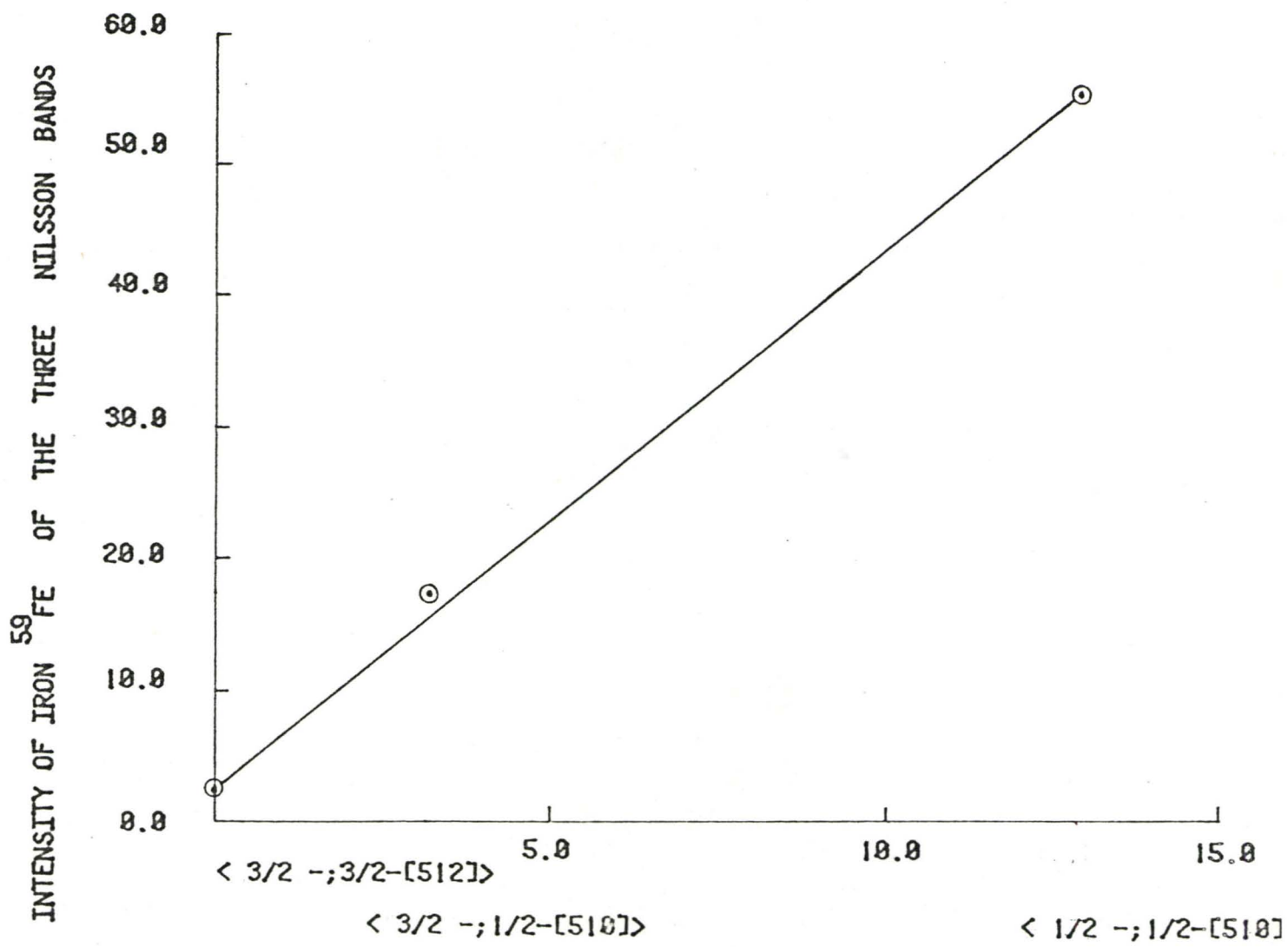


Figure 5.2 PLOT OF INTENSITY IN ⁵⁹FE V_s AVERAGE INTENSITY IN THE NILSSON BAND OF ¹⁸³W, ¹⁸¹Hf and ¹⁷⁹Hf.

CHAPTER 6

CONCLUSIONS

In this present work the energies of gamma rays from the $^{58}\text{Fe}(n,\gamma)^{59}\text{Fe}$ reaction were measured accurately using a neutron capture γ -ray pair spectrometer. The values obtained agree with the existing values in the literature. The values as obtained in this work agree well within experimental error with those of J.C. Wells, Jr.⁽¹⁰⁾ These values are more reliable than those obtained from thermal (n,γ) reaction previously reported. The detectors used in the present work have resolution which is a factor of five times better than that used in the previous investigation of the thermal (n,γ) reaction. The only handicap is the size of the sample and unfortunately, ^{58}Fe has a very low capture cross section. With a larger sample, more counts could be acquired and less statistical error would be introduced. More peaks could also develop. Examples are peaks with 3413 keV and 3130 keV which could not be established because of statistical uncertainty. Furthermore, if the reactor power is also higher than

the one used in this experiment, the time to acquire enough counts will be relatively small and the problem involved during the experiment, particularly the drifting of gain, would not be encountered.

The four sets of cascades obtained together with the accurately determined energy of the gamma rays corresponding to the transitions to the ground state, make it relatively easy to determine the neutron separation energy. This value agrees well with those obtained by A. P. Bagdanov et al.⁽⁷⁾ and fairly well with the adopted value indicated in the nuclear data sheet (34). This work confirms the value of A.P. Bagdanov⁽⁷⁾ and that the neutron separation energy is 6582.44 ± 0.42 keV.

The relative intensities of the transitions observed from the $^{58}\text{Fe}(n,\gamma)^{59}\text{Fe}$ reaction were measured. These values are in good agreement with those in the literature, particularly the one published by A.P. Bagdanov et al.⁽⁷⁾.

The ratio of capture cross section in iron isotopes ^{56}Fe and ^{58}Fe was calculated to be 2.69 ± 0.16 . This is higher than the value deduced from the literature.

This value is 2.29 ± 0.23 and means that either the $\sigma_{58\text{Fe}}$ is higher than 2.63 b given in the literature, or $\sigma_{56\text{Fe}}$ is smaller than 1.15 b given in the literature. The estimated error in this present work is less than the error associated with the cross section values given in the literature.

Correlation of the $^{58}\text{Fe}(n,\gamma)^{59}\text{Fe}$ reaction with the (d,p) reaction that was investigated shows a distinct anti-correlation between the two reactions. This is consistent with the report by A.P. Bogdanov et al.⁽⁷⁾. Furthermore, it is interesting to note that the 726.94 keV level of $3/2^-$ is a rotational excitation built on the 287.71 keV intrinsic excitation of $1/2^-$ level. They are both identified as $1/2^- [310]$ Nilsson band.

REFERENCES

1. A. Sperduto and W.W. Buechner, Phys. Rev. 134, B142 (1964).
2. E.D. Klema, L.L. Lee, Jr. and J.P. Schiffer, Phys. Rev. 161, 1134 (1967).
3. F.W. Walker, G.J. Kirovac and F.M. Rourke. Chart of the Nuclides, 12, 23 (1977).
4. S.F. Mughahghab and D.I. Garber, BNL-325 Third Edition, Neutron Cross Sections, vol. 1 (1973).
5. K.C. McLean, S.M. Dalglish, S.S. Ipson and G. Brown, Nucl. Phys. A 191, 417 (1972).
6. A.P. Bogdanov, A.V. Soroka, V.N. Thadeush and E.I. Firsov, IZV. AN BSSR, ser. fiz. - mat. nauks, 1275 (1967).
7. A.P. Bogdanov, U.A. Knatko, A.V. Soroka and V.N. Thadeush, Sov. J. Nucl. Phys. 14, 509 (1972).
8. E.K. Warburton, J.W. Olness, A.M. Nathan and J.J. Kolata, Phys. Rev. 16, 1027 (1977).
9. R. Vennink, W. Ratynski and J. Kopecky, Nucl. Phys. A 299, 429-441 (1978).
10. J.C. Wells, Jr., S. Raman and G.G. Slaughter, Phys. Rev. C 18, 707 (1978).
11. D.E. Alburger, Nucl. Instr. and Meth. 136, 323-330 (1976).
12. R.L. Walker, East Lansing, MI; Michigan State University (1975), 127p. University Microfilms Order No. 75-20,000. Thesis (Ph.D.).

13. M.A. Kaplan, R.I. Gabuniya and N.S. Androsov, pp. 82-86 of Radiatsionnaya Meditsina. erkgauf V.G. (ed). Moscow; Atomizdat (1972).
14. R.C. Greenwood and J.H. Reed, Am. Nucl. Soc. Trans. 6, 176 (1963).
15. R. Henkelmann, H.J. Born, J. Radioanal. Chem. 16, 473 (1973).
16. G.E. Thomas, D.C. Blatchley and L.M. Bollinger, Nucl. Instr. and Meth. 56, 325 (1967).
17. L. Nichol, A.M. Lopez, A. Robertson, W.V. Prestwich and T.J. Kennett, A Versatile Tangential Irradiation Facility, Nucl. Instr. and Meth. 81, 263 (1970).
18. P.M. Brewster, Thermal Neutron Capture in Selenium, Ph.D. Thesis, McMaster University, Physics Dept. (1979).
19. M.S. Patterson, Elemental Analysis with Neutron Capture Gamma Rays. M.Sc. Thesis, McMaster University, Physics Dept. (1976).
20. H. Hall, Rev. Phys. 8, 358 (1936).
21. Richard H. Pehl, Physics Today 50, Nov. (1977).
22. O. Klein, Y. Nishina, Z. Physik 52, 853 (1929).

23. A. Robertson, G.C. Cormick, T.J. Kennett and W.V. Prestwich, Nucl. Instr. and Meth. 127, 373 (1975).
24. H.J. Fiedler, L.B. Hughes, T.J. Kennett, W.V. Prestwich and B. Wall, Large Volume Lithium Drifted Germanium Ray Detectors, Nucl. Instr. and Meth. 40, 229 (1966).
25. A.H. Colenbrander and T.J. Kennett, Nucl. Instr. and Meth. 116, 251-265 (1974).
26. R. Gunnink, R.A. Meyer, J.B. Niday and R.P. Anderson, Nucl. Instr. and Meth. 65, 26 (1968).
27. A.H. Wapstra, in Proc. 2nd. Int. Conf. on Neutron Capture Gamma Ray Spectroscopy and related topics. Petten, The Netherlands (Sept. 1974).
28. R.C. Greenwood and R.G. Helmer, Nucl. Instr. and Meth. 121, 385 (1974).
29. B.N. Taylor, W.H. Parker and D.N. Laugerberg, Rev. Mod. Phys. 41, 375 (1969).
30. A. Robertson, W.V. Prestwich and T.J. Kennett, Nucl. Instr. and Meth. 100, 317-324 (1972).
31. T.J. Kennett, Private Communication.
32. M.A. Islam, S.A. Kerr, T.J. Kennett and W.V. Prestwich, A Self Consistent Set of Neutron Separation Energies, accepted for publication Can. J. Phys. (1979).

33. P.R. Bevington, Data reduction and error analysis for the Physical Sciences, McGraw Hill Book Co. (1969).
34. Nucl. Data Sheets, 19, 4 & 5 (1976).
35. M.L. Stelts and R.E. Chrien, Nucl. Instr. and Meth. 155, 253 (1978).
36. P.C. Sood, Phys. Rev. 179, 1100 (1969).
37. R.C. Pardo, C.N. Davids, M.J. Murphy, E.B. Norman and L.A. Parks, Phys. Rev. C 16, 370 (1977).
38. A.I. Namenson, H.E. Jackson and R.K. Smither, Phys. Rev. 146, 844 (1966).
39. G.A. Bartholomew, J.W. Knowles and P.J. Campion, Atomic Energy Commission of Canada, Ltd., Report No. AECL-954-43 (1960).
40. R.R. Spencer, K.T. Kaler and D.R. Dixon, Bull. Am. Phys. Soc. 11, 336 (1966).
41. M.J. Martin, J.A. Harvey and G.G. Slaughter, Bull. Am., Phys. Soc. 11, 336 (1966).